# Copyright Warning & Restrictions

The copyright law of the United States (Title 17, United States Code) governs the making of photocopies or other reproductions of copyrighted material.

Under certain conditions specified in the law, libraries and archives are authorized to furnish a photocopy or other reproduction. One of these specified conditions is that the photocopy or reproduction is not to be "used for any purpose other than private study, scholarship, or research." If a, user makes a request for, or later uses, a photocopy or reproduction for purposes in excess of "fair use" that user may be liable for copyright infringement,

This institution reserves the right to refuse to accept a copying order if, in its judgment, fulfillment of the order would involve violation of copyright law.

Please Note: The author retains the copyright while the New Jersey Institute of Technology reserves the right to distribute this thesis or dissertation

Printing note: If you do not wish to print this page, then select "Pages from: first page # to: last page #" on the print dialog screen

NJIT
New Jersey's Science &
Technology University

The Van Houten library has removed some of the personal information and all signatures from the approval page and biographical sketches of theses and dissertations in order to protect the identity of NJIT graduates and faculty.

# ABSTRACT

## RADIATIVE PROPERTIES OF SILICON RELATED MATERIALS

by

**Scott Sanowitz**

The objective of this thesis is to study the optical properties of silicon, as a function of temperature, in the infrared range of wavelengths. The wavelength range, considered in this study, is between 1 micron and 20 microns. The temperature range observed is from 50 degrees Celsius to 1000 degrees Celsius. Varying wafer thickness and doping are taken into account. The thickness of the native oxide, silicon dioxide, must be taken into account as well as its orientation (front side versus back side). The effect of layering wafers one onto another is investigated. It is shown that all these parameters affect the optical properties, emittance, reflectance, and transmittance, of a wafer and multiple layers of wafers.

The IR-563 Blackbody source is utilized as the infrared source. Emissivity measurements are performed using an Ex-Series FLIR camera and a Laser Grip -Model 1022. A matrix method based approach is implemented to simulate the optical properties.

# RADIATIVE PROPERTIES OF SILICON RELATED MATERIALS

by

Scott Sanowitz

A Thesis
Submitted to the Faculty of
New Jersey Institute of Technology
and Rutgers State University New Jersey- Newark
in Partial Fulfillment of the Requirements for the Degree of
Master of Science in Applied Physics

Federated Department of Physics

May 2016

Blank Page

## APPROVAL PAGE

## RADIATIVE PROPERTIES OF SILICON RELATED MATERIALS

**Scott Sanowitz**

---

Dr. N.M. Ravindra, Thesis Advisor Date
Professor of Physics and Director of Materials Science and Engineering Program, NJIT

---

Dr. Cristiano L. Dias, Committee Member Date
Assistant Professor, Department of Physics, NJIT

---

Dr. Keun H. Ahn, Committee Member Date
Associate Professor, Department of Physics, NJIT

## BIOGRAPHICAL SKETCH


**Author:** Scott Sanowitz


**Degree:** Master of Science

**Date:** May 2016

**Undergraduate and Graduate Education:**

- Master of Science in Applied Physics, New Jersey Institute of Technology, Newark, N.J, 2016
- Bachelors of Science in Physics, Muhlenberg College, Wescoe School, Allentown, P.A, 2013
- Bachelors of Art in Music, Muhlenberg College, Allentown, P.A, 2011

**Major:** Applied Physics

This thesis is dedicated in memoriam to Myles A. Sanowitz

# ACKNOWLEDGEMENT

The author would like to express sincere gratitude toward Dr. N.M Ravindra for his guidance and wisdom. His encouragement and determination for research was of great assistance to the author. The author has greatly benefited from technical discussion with Dr. Ravindra during this research.

The author would also like to thank Dr. Cristiano L. Dias and Dr. Keun H. Ahn for serving as committee members. The author would like to thank his, brother, mother and father for all their love and support. The author would also like to thank colleagues Ashvin Kumar Vasudevan and Sita Rajyalaxmi Marthi for offering encouragement and sharing their immense knowledge of research techniques. The author would like to give his blessings towards the "family" for all their help.

TABLE OF CONTENTS


| Chapter | | Page |
|---|---|---|
| 1 | INTRODUCTION………………………………………………………. | 1 |
| 2 | THEORETICAL BACKGROUND……………………………………..... | 4 |
| | 2.1 History of Thermography……………………………………….. | 4 |
| | 2.2 Blackbody Radiation……………………………………………….. | 6 |
| | 2.3 Greybody Radiation………………………………………………... | 12 |
| | 2.4 Basic Optical Properties…………………………………………... | 15 |
| 3 | FUNDAMENTALS OF SEMICONDUCTORS……………………… | 26 |
| | 3.1 Characteristics of Semiconductors…………………………..... | 26 |
| | 3.2 Properties of Silicon……………………………………........... | 33 |
| 4 | THERMOCOUPLES………………………………………….......... | 35 |
| | 4.1 Thermocouple Theory……………………………………………... | 35 |
| 5 | EXPERIMENTAL METHODS AND DATA ANALYSIS……………..... | 43 |
| | 5.1 Calibration via a Blackbody Source……………………………... | 43 |
| | 5.2 Multi-Rad……………………………………………………….... | 53 |
| | 5.3 Simulation of Two Wafers with Different Thin Film Layers……. | 55 |
| | 5.4 Simulation of SIMOX…………………………………………..... | 64 |
| | 5.5 Literature Review………………………………………………... | 73 |
| 6 | CONCLUSION………………………………………………………. | 75 |

## TABLE OF CONTENTS
## (Continued)

**Chapter** **Page**

REFERENCES…………………………………………………………… 76

## LIST OF TABLES

| Table | | Page |
|---|---|---|
| 2.1 | Common Materials' Emissivity Corresponding to Various Temperatures ……………...................................................... | 14 |
| 2.2 | Optical Constants for Some Materials at λ = 600nm………….... | 17 |
| 3.1 | Partial Periodic Table with Semiconductors……………………. | 26 |
| 3.2 | Energy Gaps for Some Group IV Elements at 0K………………. | 33 |
| 4.1 | Voltage Change vs. Temperature Rise (Seebeck Coefficient) for Various Thermocouple Types at 25 $^{o}$C………………………. | 37 |
| 5.1 | FLIR Camera Where the Emissivity is Set to 0.7 and Laser Grip Model 1022 Where the Emissivity is Set to 0.7 Temperature Readings for a 150mm Silicon Wafer with an Oxide Thickness of 110nm and a Mass of 4.01g……………….. | 44 |
| 5.2 | Temperature Measurements of Wafer #1 and Wafer #2 Separately Wafer #1 is a 0.7 mm Silicon Wafer with a 208µm Layer of Native Oxide ($SiO_2$) Wafer #2 is a 0.7mm Silicon Wafer with a 419µm Layer of Native Oxide…………………… | 48 |
| 5.3 | Wafers #1 and #2 in Alignment with Measurements Taken with Respect to their Front and Back Sides………………………….. | 50 |

## LIST OF FIGURES


| Figure | | Page |
|---|---|---|
| 2.1 | Shows the bands of the electromagnetic spectrum at their respective wavelengths……………………………………………… | 6 |
| 2.2 | Shows the curves of spectral radiation, sometimes called intensity versus wavelength in microns. The wavelengths traverse through the infrared, visible, and ultraviolet bands. These curves are referred to as Planck's curves…………………. | 9 |
| 2.3 | Refraction of a light beam traversing a boundary from an optically rarer medium to an optically denser medium…………………........... | 15 |
| 2.4 | Example of a damped oscillation. One can see that the amplitude is decreasing exponentially………………….............................. | 21 |
| 3.1 | Shows the impurity, phosphorous, added to crystalline silicon along the lattice. The addition of phosphorous and its subsequent substitution of a silicon atom in the silicon lattice makes the silicon n-type……………………………………………………………….. | 28 |
| 3.2 | Shows the impurity of boron added to crystalline silicon along the lattice. The addition of boron and its subsequent substitution of a silicon atom in the silicon lattice makes the silicon p-type………… | 29 |
| 3.3 | Shows the difference in band structure between metals, semiconductors and insulators. One can see the band gap increasing from metals, where it is non-existent, to semiconductors, to the largest band gap given by insulators…….. | 30 |
| 3.4 | (a) shows a direct energy band gap for a semiconductor. (b) shows an indirect energy band gap for a semiconductor………... | 32 |
| 4.1 | An example of a typical thermocouple circuit…………....................... | 35 |
| 4.2 | A circuit diagram describing a thermocouple in a voltmeter circuit………………………………………………………………... | 38 |
| 4.3 | A circuit diagram describing a thermocouple in a potentiometer circuit………………………………......................................... | 39 |
| 5.1 | Shows the experimental setup with the IR -563 Blackbody Source and clamping apparatus……………………………………………... | 45 |
| 5.2 | Shows three different (a, b, c) infrared images obtained by the FLIR camera……………………………………………………….. | 46 |

## LIST OF FIGURES
## (Continued)


| Figure | | Page |
|---|---|---|
| 5.3 | Shows both wafers' temperature measurements, front side and back side………………………………………………………… | 49 |
| 5.4 | Shows the both wafers in alignment with each other's temperature measurement. There is a greater difference in temperature between the FLIR camera's readout of the Blackbody and the single wafer versus the camera's readout of the Blackbody and the layered wafers……….............................. | 51 |
| 5.5 | Shows the Reflectance of two Silicon wafers (a) with 10nm $SiO_2$ oxide layer and (b) with 10 nm $Si_3N_4$ at 650 $^oC$…………………….. | 56 |
| 5.6 | Shows the Reflectance of two silicon wafers (a) 1000nm $SiO_2$ oxide layer and (b) 1000nm $Si_3N_4$ nitride layer…………………….. | 57 |
| 5.7 | Shows the Transmittance for two wafers (a) 10nm $SiO_2$ oxide layer and (b) 10nm $Si_3N_4$ nitride layer……………………………… | 58 |
| 5.8 | Shows the Transmittance for two wafers (a) 1000nm $SiO_2$ oxide thickness and (b) 1000nm $Si_3N_4$ nitride thickness………………… | 59 |
| 5.9 | Shows Emittance for various $SiO_2$ oxide thicknesses of (a) 10nm (b) 30nm (c) 50nm and (d) 1000nm………………………………… | 62 |
| 5.10 | Shows Emittance for various $Si_3N_4$ thicknesses of (a) 10nm (b) 30nm (c) 50nm and (d) 1000nm…………………………………….. | 63 |
| 5.11 | Shows Emittance for both wafers with layers of, (a) $SiO_2$, and (b) $S_3N_4$ at 1000nm thickness…………………………………………… | 64 |
| 5.12 | Shows the Reflectance of front side vs. backside of SIMOX at: (a) 30$^o$C, (b) 650$^o$C and (c) 1300$^o$C………................................. | 67 |
| 5.13 | The Transmittance of front side and back side of SIMOX at: (a) 30$^o$C, (b) 650$^o$C and (c) 1300$^o$C. Note the transmittance range in (b) from 0-0.18…………………………………………………….... | 68 |
| 5.14 | The Emittance of front side and back side of SIMOX at: (a) 30$^o$C, (b) 650$^o$C and (c) 1300$^o$C…………………….......................... | 70 |
| 5.15 | Sato's emissivity curves at different temperatures……………...... | 74 |

# CHAPTER 1

# INTRODUCTION

In the semiconductor industry, the two most crucial aspects for consideration are increased dimensions of the substrate and reduced device size. It is now more important than ever to minimize the temperature-time product, also known as the thermal budget, the process induced contamination, and the device failure. A number of processes have been developed that follow these guidelines, such as. Rapid Thermal Processing (R.T.P), Rapid Thermal Chemical Vapor Disposition (R.T.C.V.D), and Metal Organic Molecular Beam Epitaxy (M.O.M.B.E). In semiconductor device manufacturing, the most important process parameter is temperature. Even a slight change in temperature can result in a drastic altercation to the rate of the process. In order to properly produce a thermal model of R.T.P, one requires an understanding of the thermal properties of the material. Most of the processing in R.T.P occurs by radiation. Proper knowledge of the emissivity, reflectance and transmittance, in relation to the incident radiation of the wafer, is required. The behavior of the radiative properties of the materials under various temperatures must be accounted for.

The basic requirement of an RTP process is that the actual time-temperature profile must closely follow the specified one, and that uniformity must be maintained in steady-state at the target temperature as well as during transients. Failure to exercise such control results in undesirable effects such as

the introduction of defects in the bulk wafer, and process variations. The main problem with the conventional equipment, used in manufacturing today, lies with the approach where optimal steady-state temperature uniformity for one set of process conditions is used to design the hardware geometry, leaving only one input variable, the lamp power, for control [1]. The lamp power for RTP is the point source for radiation. The lamp is of the tungsten-halogen variety.

This thesis will investigate the optical properties of silicon, particularly in the infrared range of wavelengths. The parameter of temperature and wavelength will be taken into account. The optical properties in the infrared range of the electromagnetic spectrum, from 1 to 20 microns, are investigated. Varying wafer thickness and doping effects are considered in this study. The addition of multilayers is considered in the modeling. The following case studies are considered here: silicon dioxide on silicon; silicon nitride on silicon; thickness and front side versus back side; wafer orientation; silicon on silicon dioxide on silicon, also known as SIMOX (Separation by IMplanted OXygen), as well as SIMOX's front side versus back side.

The infrared source, utilized in the experiment, was an IR-563 Blackbody source. This source generates radiation in the visible as well as infrared spectrum (the spectrum of interest in RTP). The interaction of the radiation with silicon is imaged using an FLIR camera and a Laser-Grip Model 1022. A matrix method based approach was implemented to simulate the optical properties of the various materials.

Over the next six chapters, the various parameters of wavelength, temperature and material will be explored. Chapter 2 presents the history and fundamentals of Blackbody radiation and Greybody radiation. An overview of the optical properties will be discussed as well as their relation to thermal properties. Chapter 3 will discuss general semiconductor fundamentals with a concise focus on silicon. Chapter 4 will discuss thermocouples and their implementation in processing. Chapter 5 will feature the experimental setup, simulation, and data interpretation. Chapter 6 will conclude with the findings of this research.

# CHAPTER 2

# THEORETICAL BACKGROUND

## 2.1 History of Infrared Technology

Like a number of great scientific discoveries, the infrared spectrum was discovered by accident. It was discovered in 1800 by Sir William Herschel, the Royal Astronomer to King George III who was already famous for his discovery of the planet Uranus. He was searching for optical filters which would reduce the brightness of the sun's image during solar observations. While trying out different materials, he was astounded to find that some samples passed very little of the sun's heat while others passed so much heat that it would damage the eye in a mere few seconds. Hershel needed to find a material that would reduce the brightness of the sun while also obtaining a maximum reduction in heat. He conducted an experiment. The experiment was conducted wherein he blackened mercury in a glass thermometer with ink and began to test the heating effects of various colors of the spectrum formed by sunlight passing through a glass prism. As the blackened thermometer slowly moved across the color spectrum, the temperature readings showed a steady increase from the violet end to the red end. When Herschel moved the thermometer into the dark regions beyond the red end of the spectrum, it showed an increase in temperature. Herschel knew that there

must be a point where the heating effect was maximized and this point was way beyond the red end of the spectrum. This is known today as infrared wavelengths.

Any experiment must overcome the strict scrutiny of the scientific community. Many of Herschel's contemporaries tried using different glasses as prism to confirm the infrared spectrum. Different glasses will provide different transparencies for the infrared. In 1830, an Italian named Macedonio Melloni discovered that when rock salt (NaCl) was made into lenses and prisms, it was extremely transparent to the infrared spectrum. Rock salt was to remain the principle infrared optical material until synthetic crystal growing was mastered by 1930.

In 1829, Leopoldo Nobili invented the thermocouple. Melloni connected a bunch of thermocouples together to create a thermopile. The thermopile was 40 times as sensitive as the best thermometer of the day and could sense the heat from a person from three meters away. In 1840, Sir John Herschel, son of Sir William Herschel, developed a way to image the infrared spectrum. He used a thin film of oil that would evaporate when a heat pattern was focused on it. The thermal image could be seen by the reflecting light where the interference effects of the oil made the thermal image visible to the eye. In 1880, Samuel Pierpont Langley invented the bolometer. The bolometer consisted of a thin blacked strip of platinum connected to a Wheatstone bridge circuit upon which infrared radiation was focused to a responsive galvanometer. The bolometer was said to detect heat from a cow from 400 meters away. Between 1900 and 1920, many patents were issued for devices that detected infrared. The military was especially interested in being

able to “see in the dark” and in developing torpedo guidance systems. In between World War I and II, the military did the foremost research on infrared applications. The image converter was invented and let soldiers see in the dark. Since the 1950’s, the military’s grasp of infrared research has been elevated and thermal imaging devices are available for civilian use today [2].

## 2.2 Blackbody Radiation

All radiation is in fact part of the electromagnetic spectrum. The spectrum is divided into arbitrary wavelength regions known as bands. They were historically split up into bands based on the method of detection. All the bands follow the same laws as each other and only differ in wavelength.

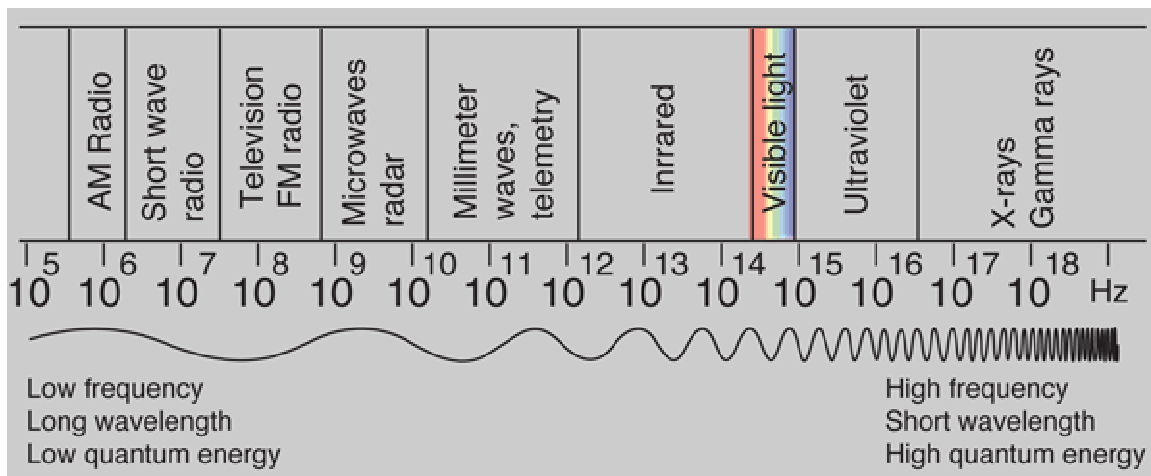


**Figure 2.1** Shows the bands of the electromagnetic spectrum at their respective wavelengths.
Source: [3].

The study of infrared thermal imaging is known as thermography. At the short wavelength end of the infrared spectrum lies a deep red color of light, while the long wavelength end lies in the blurred space merging towards microwave radio wavelengths, in the millimeter range. Further divided lines are made in the infrared spectrum into four sub-bands. They are known as the near infrared, 0.75-3 μm; middle infrared, 3-6μm; far infrared, 6-15μm; and extreme infrared, 15-100μm. These measurements are expressed in microns, μm, but wavelength measures are commonly found in nanometers, nm, and Angstroms, Å.

A blackbody is defined as an object which absorbs all incident radiation at all wavelengths. Kirchhoff's law states that a body capable of absorbing all radiation at any wavelength is equally capable in the emission of radiation.

$$\alpha_\lambda = \varepsilon_\lambda \tag{2.1}$$

Stating the absorptivity, $\alpha_\lambda$, equals the emissivity, $\varepsilon_\lambda$. The construction of blackbody source consists of an aperture in an isotherm cavity. The cavity does not change in temperature and is made of an opaque absorbing material. The material is placed into a box that is light tight except for the aperture which is placed on one side of the box. All radiation that enters the hole is scattered and absorbed repeatedly by reflections, so that only an infinitesimal amount of radiation can escape. The blackness at the aperture is nearly equal to that of an ideal blackbody and is almost perfect for all wavelengths.

Radiant flux is the energy from the electromagnetic radiation that is emitted, reflected, transmitted or received, per unit time.

$$\Phi_e = \frac{\partial Q}{\partial t} \tag{2.2}$$

where $\Phi_e$ is the radiant flux, Q is the electromagnetic energy and t is the time. Spectral flux is the radiant flux over wavelength or frequency.

$$\Phi_{e,\lambda} = \frac{\partial \Phi_e}{\partial \lambda} \tag{2.3}$$

where $\Phi_{e,\lambda}$ is the spectral flux, $\Phi_e$ is the radiant flux and λ is the wavelength. λ, wavelength can be replaced by $\nu$, the frequency [4]. When scientists, in the late $19^{th}$ to early $20^{th}$ century, started plotting the spectral flux, they produced a graph with perplexing curves.

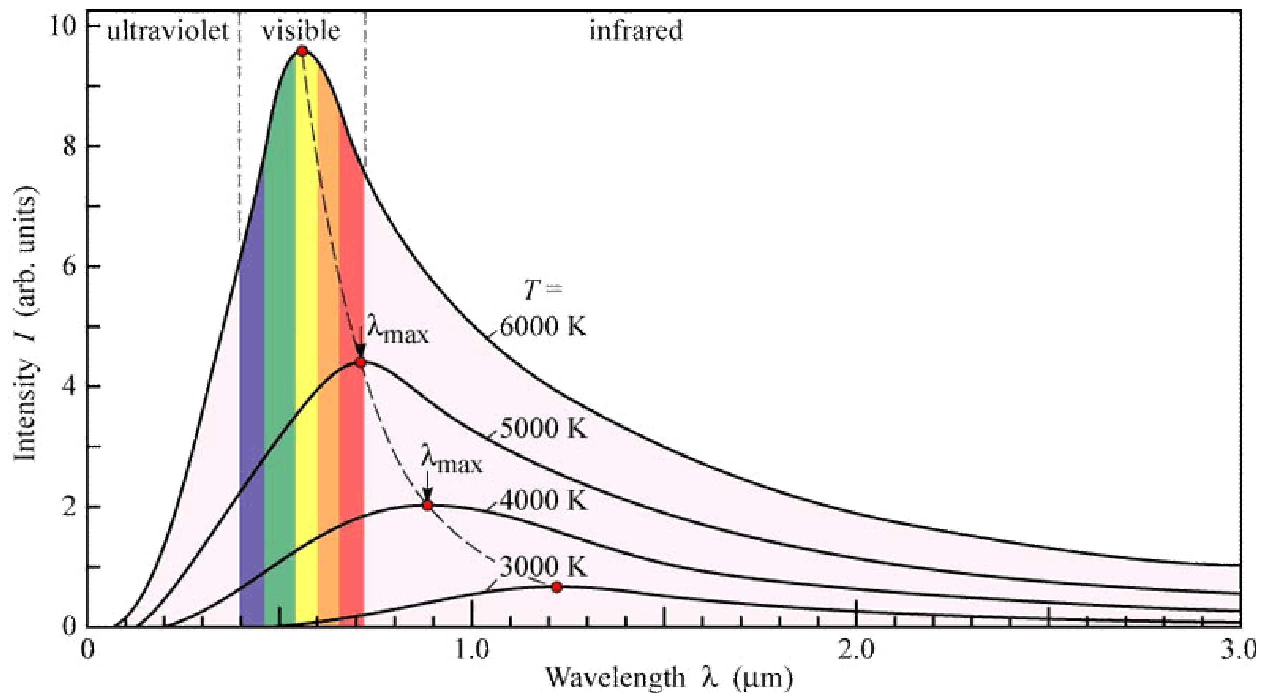


**Figure 2.2** Shows the curves of spectral radiation, sometimes called intensity versus wavelength in microns. The wavelengths traverse through the infrared, visible, and ultraviolet bands. These curves are referred to as Planck's curves. Source: [5].

At first, the scientists at that time could not come up with the equations governing these curves. In 1896, Wilhelm Wien proposed an equation to model the spectral flux of a blackbody:

$$I(\nu, T) = \frac{2h\nu^3}{c^2} e^{\left(\frac{h\nu}{kT}\right)} \quad (2.4)$$

where, I(ν,T) is the amount of energy per unit surface area, time, solid angle and frequency, ν. T is temperature, h is Planck's constant, k is Boltzmann's constant and c is the speed of light. This was a good approximation of spectral flux, but only

for short wavelength and hence high frequencies. In 1905, Lord Rayleigh and Sir James Jeans proposed an equation that fit the curves of the spectral flux for a blackbody at long wavelengths.

$$W_{\lambda b} = \frac{2ckT}{\lambda^4} \tag{2.5}$$

$W_{\lambda,b}$ is the spectral flux of a blackbody. This law, besides not fitting the curves for all wavelengths, has another devastating consequence. It predicted infinitely small wavelengths and approached zero as the energy emitted would approach infinity. This was known as the ultraviolet catastrophe for Rayleigh-Jeans law. It would start to diverge from the spectral flux curves starting in the ultraviolet regions of the electromagnetic spectrum [6]. It was not until Max Planck quantized light into so called packets of radiation we now call photons that an accurate equation could describe the spectral flux curves for a black body:

$$W_{\lambda,b} = \frac{2\pi hc^2}{\lambda^5\left(\exp\left(\frac{hc}{\lambda kT}\right)-1\right)} * 10^{-6} \ \left[\frac{W}{m^2}\right](\mu m) \tag{2.6}$$

where $W_{\lambda,b}$ is spectral emittance, c is the velocity of light, h is Planck's constant, k is Boltzmann's constant, T is temperature, and λ is wavelength in microns. Equation 2.6 accurately describes the family of curves seen in Figure 2.2. This is

known as Planck's law and works for all range of wavelengths. We can see in Figure 2.2 that when the wavelength is zero, the spectral emittance is also zero. As the wavelengths increase slightly, the spectral emittance increases rapidly until it reaches a maximum at $\lambda_{max}$. For very long wavelengths, the spectral emittance approaches zero. An intriguing aspect of the curves is the $\lambda_{max}$, where the spectral emittance is at its highest value. The $\lambda_{max}$ occurs at shorter wavelengths for higher temperature.

By differentiating Planck's formula with respect to λ and finding the maximum, one obtains Wien's displacement law.

$$\lambda_{max} = \frac{2898}{T} (\mu m) \tag{2.7}$$

This formula is useful for describing a well-known phenomenon that, as the temperature of a thermal radiator increases, it will change colors from red to orange to yellow. A very hot star such as Sirius has a temperature of approximately 11,000 K. Upon observation, it emits a bluish-white light. This star's peak spectral radiance occurs in the ultraviolet spectrum at a wavelength of 0.27 μm. Our sun has a surface temperature of about 6,000 K and emits a yellow light. Its peak spectral emittance occurs in the middle of the visible spectrum with a wavelength at about 0.5 μm. At room temperature, i.e. 300 K, the peak spectral emittance occurs at 38 μm which is considered to be in the far infrared.

By integrating Planck's formula from a wavelength of $\lambda = 0$ to $\lambda = \infty$, the total radiant emittance can be obtained.

$$W_b = \sigma T^4 \left[\frac{W}{m^2}\right] \quad (2.8)$$

This is Stefan-Boltzmann's law. Here, $W_b$ is the total radiant emittance, σ is the Stefan-Boltzmann constant and T is the temperature in Kelvin. Graphically, like any integral, it represents the area under a curve. This curve in this instance is the Planck curve and Stefan-Boltzmann's law calculates the area under it. When calculating the total emittance from $\lambda = 0$ to $\lambda = \lambda_{max}$, the total radiant emittance is only about 25%. This represents approximately the amount of the sun's radiation inside the visible spectrum.

## 2.3 Greybody Radiation

A blackbody is an idealization of radiators. Most real objects do not comply with the laws discussed previously though they may exhibit some blackbody behavior in certain wavelength ranges. There are three processes which prevent a real object from behaving like a blackbody. A percentage of the incident radiation may be absorbed, α; a percentage can be reflected, ρ; and a percentage can be transmitted, $\tau$. The sum of these factors must always add to unity at any wavelength and temperature.

$$\alpha_\lambda + \rho_\lambda + \tau_\lambda = 1 \tag{2.9}$$

For an opaque material, $\tau_\lambda = 0$ and the equation 2.9 simplifies to:

$$\varepsilon_\lambda + \rho_\lambda = 1 \tag{2.10}$$

$\varepsilon_\lambda$ is called spectral emissivity. It is the ratio of the spectral radiant power from an object to that from a blackbody at the same temperature and wavelength. This can be expressed as the spectral radiance of the object to that of the blackbody as follows:

$$\varepsilon_\lambda = W_{\lambda o}/W_{\lambda b} \tag{2.11}$$

In general, there are three types of radiators. A blackbody in which $\varepsilon_\lambda = \varepsilon = 1$, where $\varepsilon$ is the emissivity from a blackbody; a greybody for which $\varepsilon_\lambda$ is a constant less than one; a selective radiator for which $\varepsilon_\lambda$ varies at different wavelengths. For a greybody radiator, the Stefan-Boltzmann's law becomes:

$$W = \varepsilon\sigma T^4 \left[\frac{W}{m^2}\right] \quad (2.12)$$

The total emissive power from a greybody is the same as a blackbody at the same temperature and wavelength reduced in proportion to the value of ε from the greybody.

**Table 2.1** Common Materials' Emissivity Corresponding to Various Temperatures

| Material Specification | Temperature (ºC) | Emissivity |
|---|---|---|
| Aluminum foil | 27 | 0.04 |
| Aluminum sheet | 100 | 0.09 |
| Brass oxidized | 100 | 0.61 |
| Brass polished | 200 | 0.03 |
| Brick fireclay | 1000 | 0.75 |
| Brick masonry | 35 | 0.94 |
| Bronze polished | 50 | 0.1 |
| Copper polished | 100 | 0.03 |
| Copper oxidized | 20 | 0.78 |
| Gold polished | 130 | 0.018 |
| Iron and Steel polished | 100 | 0.07 |
| Iron galvanized sheet | 92 | 0.07 |
| Lead shiny | 250 | 0.08 |
| Nickel Oxide | 500-650 | 0.52-0.59 |

Source: [2].

## 2.4 Basic Optical Properties

When light passes from an optically thin medium into an optically dense medium, one observes that an angle forms between the refracted light beam and a line perpendicular to the surface. This angle is known as the angle of refraction, β. This angle of refraction is generally smaller than the angle of incidence, α, for light propagating from a rarer medium to a denser medium.

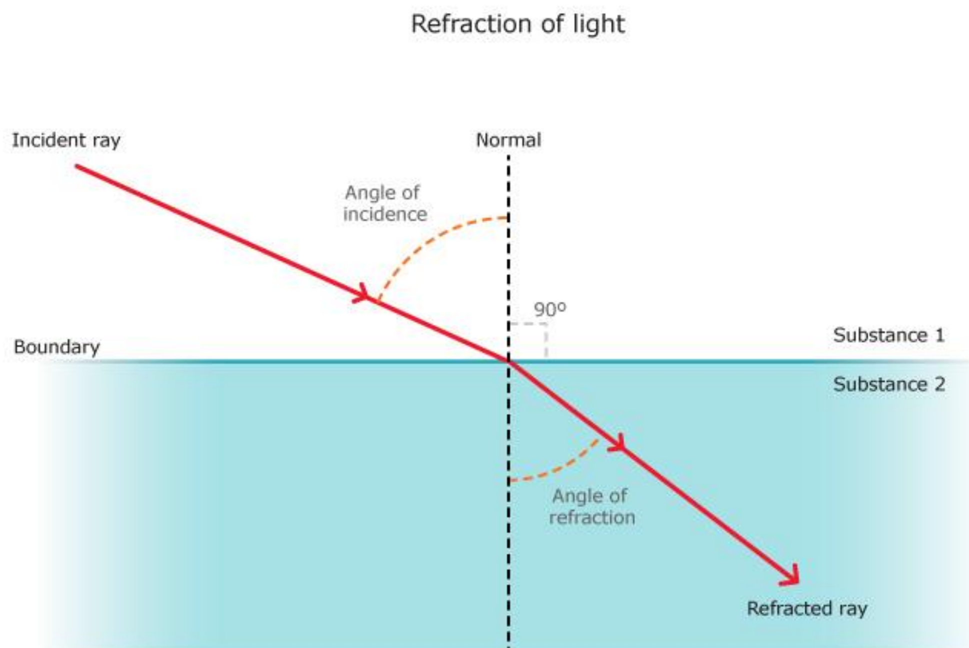


**Figure 2.3** Refraction of a light beam traversing a boundary from an optically rarer medium to an optically denser medium.
Source: [7].

This is a well-known phenomenon that is used for the definition of the refractive power of a material. It is known as Snell's law.

$$\frac{sin\alpha}{sin\beta} = \frac{n_{med}}{n_{vac}} = n \tag{2.13}$$

where n is the index of refraction. Commonly $n_{vac}$ is arbitrarily set to unity. The phenomenon of refraction is caused by the change in velocities, when traversing different mediums. Thus, if light passes from vacuum, to a different medium, we find:

$$n = \frac{c_{vac}}{c_{med}} = \frac{c}{v} \tag{2.14}$$

where v is the velocity of light of some arbitrary medium. The magnitude of the refractive index of light depends on the wavelength of the incident light. This property is known as dispersion. To summarize, when light passes from vacuum to a medium, its velocity as well as its wavelength generally decrease to keep the frequency, and thus energy, constant [8].

**Table 2.2** Optical Constants for Some Materials at λ = 600nm

| Material | n | k | W (nm) | R% |
|---|---|---|---|---|
| Copper | 0.14 | 3.35 | 14.2 | 95.6 |
| Gold | 0.21 | 3.21 | 14.7 | 98.9 |
| $Al_2O_3$ | 1.76 | $\sim 10^{-7}$ | | 7.58 |
| Quartz | 1.55 | $\sim 10^{-7}$ | $3 * 10^8$ | 4.65 |
| Polyethylene | 1.51 | $\sim 10^{-7}$ | | 4.13 |
| Polystyrene | 1.60 | $\sim 10^{-7}$ | | 5.32 |
| Silicon | 3.94 | 0.025 | 1,910 | 35.42 |
| GaAs | 3.91 | 0.228 | 209 | 35.26 |

Source: [8].

Additional constants are needed to characterize the optical properties of materials. Let us consider a plane-polarized wave that propagates along the z-direction and oscillates in the x-direction. We will negate possible effects due to magnetic fields. In this case, the electro-magnetic wave equation will read as:

$$\frac{c^2 \partial^2 \mathcal{E}_x}{\partial z^2} = \varepsilon \frac{\partial^2 \mathcal{E}_x}{\partial t^2} + \frac{\frac{\sigma}{\varepsilon_o} \partial \mathcal{E}_x}{\partial t} \tag{2.15}$$

where $\mathcal{E}_x$ is the electric field strength, ε is the dielectric constant, σ is the conductivity, and $\varepsilon_o$ is the permittivity of empty/free space. The solution of equation 2.15 is achieved using the following trial solution:

$$\mathcal{E}_x = \mathcal{E}_o \exp\left[i\omega\left(t - \frac{zn}{c}\right)\right] \tag{2.16}$$

where $\mathcal{E}_o$ is the maximal value of the electric field strength and ω = 2πν is the angular frequency. Differentiating equation 2.16 once with respect to time and twice with respect to time and z and inserting these values into equation 2.15, one obtains:

$$\check{n}^2 = \varepsilon - \frac{\sigma}{\varepsilon_o \omega} i \tag{2.17}$$

Equation 2.17 leads to an important result that the index of refraction is generally a complex number. We denote the complex index of refraction as ň. Like any complex number, it consists of two parts, a real part and an imaginary part. The imaginary part of the index of refraction is often represented by k.

$$\check{n} = n - ik \tag{2.18}$$

k is often referred to as the damping constant, absorption constant, attenuation coefficient or extinction coefficient. Values for k for some materials are given in Table 2.2.

$$\check{n}^2 = n^2 - k^2 - 2nki \quad (2.19)$$

Equating the real and imaginary parts between equations 2.17 and 2.18 yields an important relation between electrical and optical constants.

$$\varepsilon = n^2 - k^2 \quad (2.20)$$

$$\sigma = 4\pi\varepsilon_o nk\nu \quad (2.21)$$

Looking back at equation 2.17, there is a difference between two dielectric constants, a real one and an imaginary one. The dielectric constant can be rewritten as:

$$\acute{\varepsilon} = \varepsilon_1 - i\,\varepsilon_2 \quad (2.22)$$

Equating the real and imaginary parts between equations 2.22 and 2.19, we obtain:

$$\varepsilon_1 = n^2 - k^2 \tag{2.23}$$

$$\varepsilon_2 = 2nk \tag{2.24}$$

Similarly, as with the index of refraction, $\varepsilon_1$ and $\varepsilon_2$ are the real and imaginary parts of the complex dielectric constant, έ. Keep in mind that $\varepsilon_1$ is identical to ε in equation 2.20.

If we now return to the trial solution of the electric wave equation and insert the complex dielectric constant, we obtain:

$$\mathcal{E}_x = \mathcal{E}_o \exp\left[i\omega\left(t - \frac{z(n-ik)}{c}\right)\right] \tag{2.25}$$

which can be rewritten as:

$$\mathcal{E}_x = \mathcal{E}_o \exp\left[-\frac{\omega k}{c} z\right] \exp\left[i\omega\left(t - \frac{zn}{c}\right)\right] \tag{2.26}$$

Equation 2.26 represents a damped wave. This means that, in matter, the amplitude of the wave decreases exponentially with an increasing z value. The constant k determines how much the amplitude decreases, the degree of damping of the light wave.

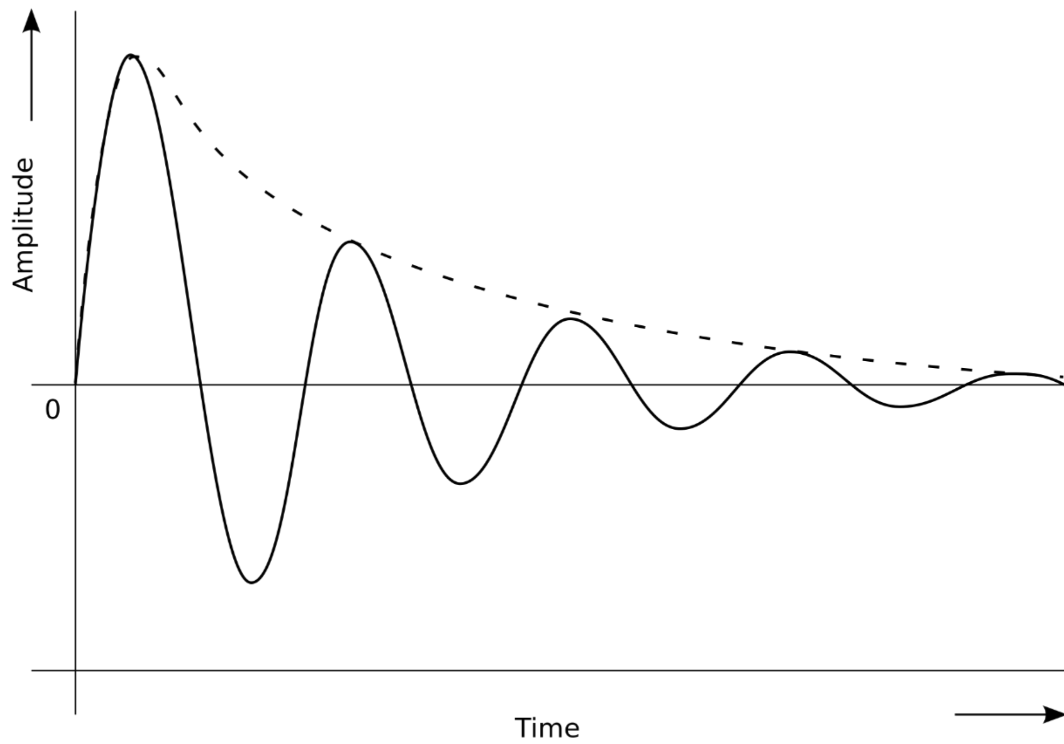


**Figure 2.4** Example of a damped oscillation. One can see that the amplitude is decreasing exponentially.
Source: [9].

The field strength, Ɛ, is difficult to measure in an experimental setting. Thus the intensity, I, can be measured effortlessly with such devices as the photodetector. The intensity equals the square of the field strength.

$$I = \mathcal{E}^2 = I_o \exp(-\frac{2\omega k}{c} z) \tag{2.27}$$

The distance at which the intensity of the light wave, which travels through a medium, has decreased by 1/e or approximately 37% is known as the characteristic penetration depth, W.

$$\frac{I}{I_o} = \frac{1}{e} \tag{2.28}$$

$$z = W = \frac{c}{2\omega k} = \frac{\lambda}{4\pi k} \tag{2.29}$$

Table 2.2 presents some values for W for light having a constant wavelength of $\lambda$ = 600 nm. The inverse of W is called absorption coefficient and is given by:

$$\alpha = \frac{4\pi k}{\lambda} = \frac{\sigma}{nc\varepsilon_o} \tag{2.30}$$

The ratio between the transmitted light intensity, $I$, and the incident light intensity, $I_o$, is known as Beer-Lambert law. It is given by:

$$\frac{I}{I_o} = \exp\left(-\frac{2\omega kz}{c}\right) = \exp(-\alpha z) \tag{2.31}$$

Not all incident light is transformed into other energy forms, such as heat, but instead may be reflected, scattered or, as above, transmitted. It should be noted that Beer-Lambert's law breaks down for substances that are highly scattering in nature.

Many materials can be categorized by the way they reflect light. For metals, light penetrates at only a short distance. Thus only a small part of the impinging energy is converted to heat. The majority of the energy is reflected. In contrast, for glass, light penetrates much farther than metals, approximately seven orders of magnitude more. As consequence, very little light is reflected by glass. However, a very thick piece of glass, about 1 to 2 meters, will dissipate the impinging energy into heat [8].

The ratio between the reflected intensity, $I_R$, and the incoming intensity, $I_o$, is known as the reflectivity. It is given by:

$$R = \frac{I_R}{I_o} \tag{2.32}$$

Similarly, the ratio between the transmitted intensity, $I_T$, and the impinging light intensity, $I_o$ is known as transmissivity, or transmittance.

$$T = \frac{I_T}{I_o} \tag{2.33}$$

Due to experimental data, the reflectivity, R, is known to only depend on values of the index of refraction, n. Generally, the index of refraction is a complex number, however, R must remain a real number, so the modulus must be taken.

$$R = \left|\frac{\check{n}-1}{\check{n}+1}\right|^2 \tag{2.34}$$

which yields:

$$R = \frac{(n-1)^2+k^2}{(n+1)^2+k^2} \tag{2.35}$$

Equation 2.35 is known as Beer's equation. Reflectivity is a dimensionless material constant and is often given in a percentage of the incoming light. Table 2.2 lists these percentages for a few materials. Like the index of refraction, reflectivity is a function of the wavelength of light, λ. Reflectivity can also be expressed as a function of $\varepsilon_1$ and $\varepsilon_2$:

$$R = \frac{n^2+k^2+1-2n}{n^2+k^2+1+2n}. \tag{2.36}$$

$$n^2 + k^2 = \sqrt{\varepsilon_1^2 + \varepsilon_2^2} \tag{2.37}$$

$$2n = \sqrt{2(\sqrt{\varepsilon_1^2 + \varepsilon_2^2} + \varepsilon_1)} \quad (2.38)$$

By substitution of 2.37 and 2.38 into 2.36, we get:

$$R = \frac{\sqrt{\varepsilon_1^2 + \varepsilon_2^2} + 1 - \sqrt{2(\sqrt{\varepsilon_1^2 + \varepsilon_2^2} + \varepsilon_1)}}{\sqrt{\varepsilon_1^2 + \varepsilon_2^2} + 1 + \sqrt{2(\sqrt{\varepsilon_1^2 + \varepsilon_2^2} + \varepsilon_1)}} \quad (2.39)$$

Thus the relationship between the complex dielectric constant and reflectivity is derived as above.

# CHAPTER 3

# FUNDAMENTALS OF SEMICONDUCTORS

## 3.1 Characteristics of Semiconductors

The study of semiconductors and their application in electronic devices has led to marvelous advances in the technology industry. Semiconducting elements can be found in column IV of the periodic table and its surrounding neighbor columns.

**Table 3.1** Partial Periodic Table with Semiconductors

| II | III | IV | V | VI |
|---|---|---|---|---|
| | B<br>Boron | C<br>Carbon | N<br>Nitrogen | |
| Mg<br>Magnesium | Al<br>Aluminum | Si<br>Silicon | P<br>Phosphorous | S<br>Sulfur |
| Zn<br>Zinc | Ga<br>Gallium | Ge<br>Germanium | As<br>Arsenic | Se<br>Selenium |
| Cd<br>Cadmium | In<br>Indium | Sn<br>Tin | Sb<br>Antimony | Te<br>Tellurium |
| Hg<br>Mercury | | Pb<br>Lead | | |

Source: [11].

Column IV represents the elemental semiconductors, silicon, Si and germanium, Ge. The elements from columns III and V, as well as the elements form columns II and VI, make up intermetallic, or compound semiconductors. The variety of semiconductor materials has given way for many designs and fabrications of electronic and optoelectronic devices. For example, germanium was used in the early days of semiconductor use for diodes and transistors. Silicon is now predominantly used for diodes, rectifiers, solar cells, transistors, memory devices and integrated circuits. The III-V compounds are used in high-speed devices requiring the emission or absorption of light. GaAs, GaN, InP and GaP are such compounds that are fabricated in the use of light emitting diodes (LEDs). Fluorescent materials such as those seen in television screens are generally the II-VI compounds, such as ZnS. Light detectors commonly consist of InSb, CdSe, or other compounds such as PbTe and HgCdTe. Silicon and germanium are also widely used as infrared and nuclear radiation detectors [11].

Materials are categorized based on their resistivity (or conversely conductivity). Insulators have a high resistivity, while metals have a low resistivity. Semiconductors have a resistivity which is in-between insulators and metals [10]. The optical and electronic properties of semiconductor materials are significantly affected by the addition of impurities. These foreign elements may be added precisely in controlled amounts. These impurities are utilized to vary the resistivity of the semiconductor. The process of the controlled addition of impurities is called doping.

There are two types of dopants found in semiconductors, n-type dopants and p-type dopants. N- type doping results in an overall negative charge to an otherwise neutral semiconductor. Each atom of the n-type dopant contributes a conduction electron giving way to excess conduction electrons and hence a net negative charge. For example, consider if silicon was doped with phosphorous. Each phosphorous atom now contributes conduction electrons making the silicon n-type.

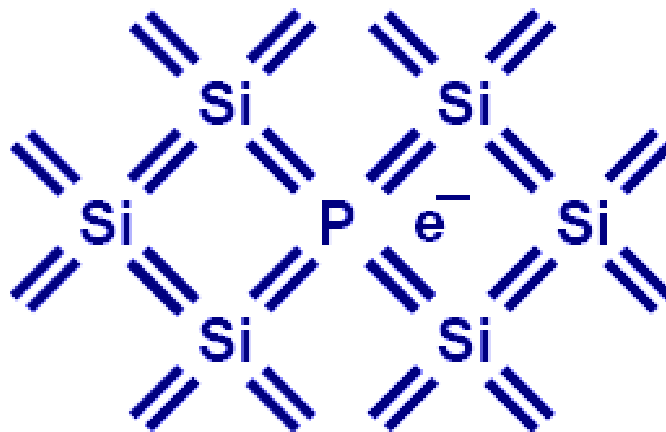


**Figure 3.1** Shows the impurity, phosphorous, added to crystalline silicon along the lattice. The addition of phosphorous and its subsequent substitution of a silicon atom in the silicon lattice makes the silicon n-type.
Source: [10].

P-type doping results in an overall positive charge to an otherwise neutral semiconductor. Each atom of the p-type dopant contributes a hole giving way to a lattice that contains more holes than conduction electrons, hence a net positive charge. For example, consider if silicon is now doped with boron. Each boron atom now contributes a hole. The number of holes will outnumber the conduction electrons making the silicon p-type.

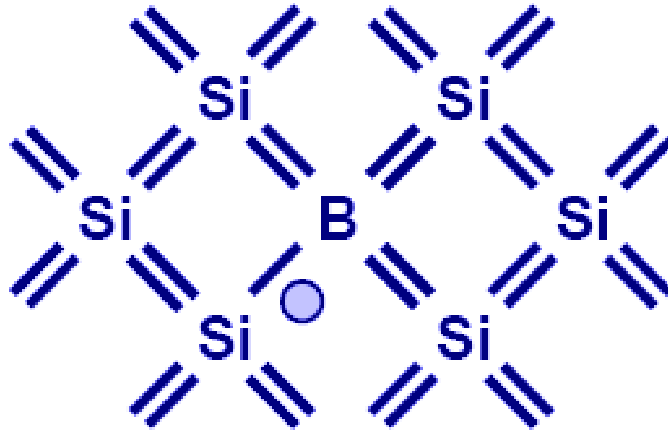


**Figure 3.2** Shows the impurity of boron added to crystalline silicon along the lattice. The addition of boron and its subsequent substitution of a silicon atom in the silicon lattice makes the silicon p-type.
Source: [10].

Another defining characteristic of semiconductors is its energy band gap. At 0K, semiconductors have the same band structure as insulators, a filled valence band separated from an empty conduction band. The difference between insulators, metals and semiconductors lies with the size of the band gap, $E_g$. $E_g$ is much smaller in a semiconductor than an insulator, while $E_g$ in a metal is non-existent for the valence band and conduction band overlap. The concentration of conduction electrons, $n_i$, depends on the band gap $E_g$, and the absolute temperature. (For intrinsic silicon)

$$n_i = 5.2 * 10^{15} \exp\left[\frac{-E_g}{2kT}\right] \; electrons/cm^3 \qquad (3.1)$$

$n_i$ is approximately 1 x $10^3$ electrons/$cm^3$ at 300K and $n_i$ is approximately 1 x $10^5$ electrons/$cm^3$ at 600K. A relatively small band gap in semiconductors allows for the excitation of electrons from the lower valence band to the upper conduction band by the proper amount of thermal or optical energy. For example, at room temperature, a semiconductor with a 1eV band gap will have a significant amount of electrons excited across the band gap into the conduction band. However, an insulator with 10eV band gap will have a negligible number of excitations [11].

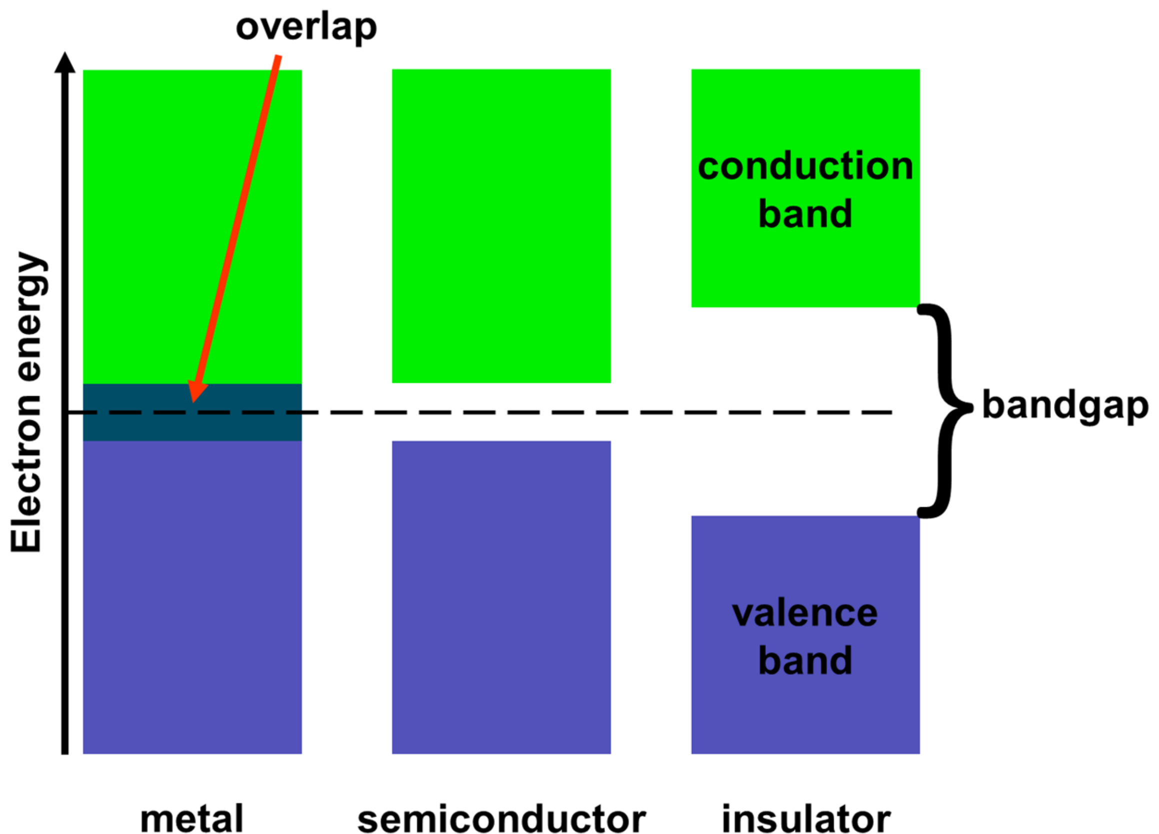


**Figure 3.3** Shows the difference in band structure between metals, semiconductors and insulators. One can see the band gap increasing from metals, where it is non-existent, to semiconductors, to the largest band gap given by insulators.
Source: [12].

At 0K, all the electrons are in the valence band of a semiconductor. As the temperature increases, some electrons are excited to the conduction band. This leaves some electrons in the conduction band and empty states in the valence band. These empty states in the valence band are referred to as holes. By the excitation of an electron from the valence band to the conduction band, a conduction electron is created and a hole forms. Conduction electrons and holes form in pairs, electron-hole pairs.

There are two classes of semiconductors both categorized by their respective band gaps. The two classes of band gaps lead to direct and indirect energy gaps. If the semiconductor has a direct band gap, the minima of the conduction curve is aligned with the maxima of the valence curve. If the semiconductor has an indirect band gap, the minima of the conduction curve does not align with the maxima of the valence curve. Some examples of indirect band gap semiconductors are silicon, AlSb, and germanium. Some direct band gaps are GaAs and InP.

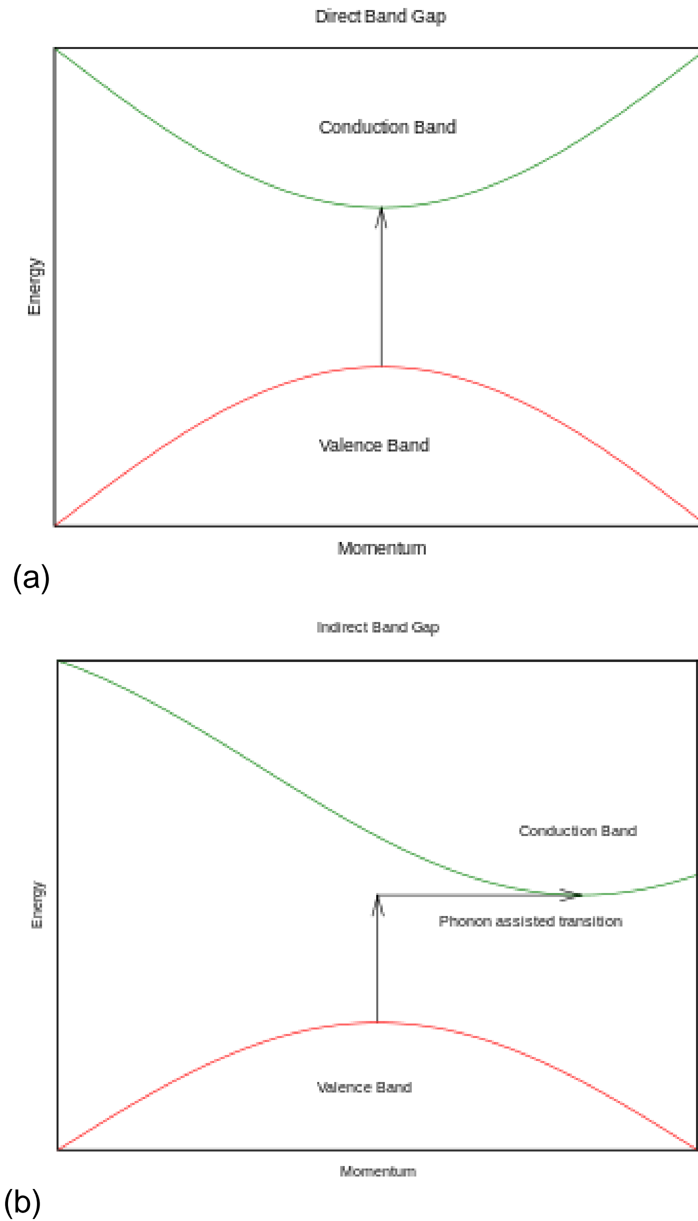


**Figure 3.4** (a) shows a direct energy band gap for a semiconductor. (b) shows an indirect energy band gap for a semiconductor.
Source: [13].

For a direct transition from the valence band to the conduction band, an electron only needs a photon to excite it. Its momentum in the lattice will remain the same. For an indirect transition, the electron will still be excited by a photon,

thus, gaining energy, but its lattice momentum will change due to a phonon propelling the electron into the conduction band.

**Table 3.2** Energy Gaps for Some Group IV Elements at 0K

| Element | $E_g$ (eV) |
|---|---|
| Carbon (diamond) | 5.48 |
| Si | 1.17 |
| Ge | 0.74 |
| Sn (gray) | 0.08 |

Source: [8].

## 3.2 Properties of Silicon

Silicon is the 14th element in the periodic table. In a single crystal form, silicon exhibits the diamond lattice structure. The atomic density of silicon is 5.2 x $10^{22}$ atoms/$cm^3$. Silicon has four valence electrons and can covalently bond to its four nearest neighbors. Pure silicon has a lattice constant of 5.43086 Å. The nearest neighbor distance between the atoms in the diamond lattice is 2.35163 Å. The intrinsic carrier concentration is about $10^{10}$ $cm^{-3}$ at 300K. The conduction electron mobility in lightly doped silicon is 1350 $cm^2$/V, while that of hole mobility is 475 $cm^2$/V at 300K. The shear stress for silicon is 3.61 x $10^7$ dyne/$cm^2$. Due to silicon's shear stress factor, it is possible for silicon to be made into 300mm and 450 mm wafers [14].

Silicon remains the semiconductor of choice for the fabrication of semiconductor devices and microcircuits. Silicon is chosen for these applications due to the fact that silicon is an elemental semiconductor. It can be subjected to a wide variety of processing steps without any concern of decomposition that is the situation with compound semiconductors. Also, silicon can be fabricated into microcircuits that are capable of high temperature operation. Silicon is available for surface passivation treatments. For instance, forming a layer of thermally grown $SiO_2$, provides the device with protection. Silicon may be utilized in the majority of the applications in the semiconductor industry, but it is not the best choice for some applications. Due to silicon's indirect band gap, many functions cannot be delivered by silicon. These include lasers, light-emitting diodes, and a variety of optoelectronic devices. Silicon in the form of silica and silicates comprises approximately 25% of the earth's crust, making it quite abundant in nature compared to other semiconducting materials.

# CHAPTER 4

# THERMOCOUPLES

## 4.1 Thermocouple Theory

Temperature is the most important process parameter in RTP and, for that matter, in most semiconductor processes. In order to measure temperature effectively and safely, a thermocouple device is utilized. Thermocouples provide a wide and useful temperature range, are inherently differentiable, are rugged, are reliable and inexpensive, and usually give a fast response. A thermocouple consists of two wires of dissimilar metals. These two wires are joined together at one end, called the measurement junction. The other end, where the wires are not joined is connected to the signal conditioning circuitry traces, typically made of copper. The junction between the thermocouple metals and the copper traces is called the reference junction [15].

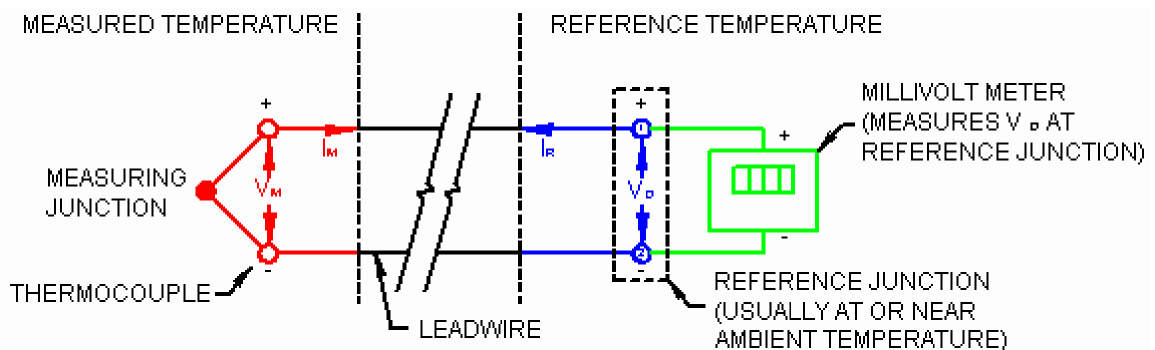


**Figure 4.1** An example of a typical thermocouple circuit.
Source: [16].

Thermocouples have advantages and disadvantages. Starting with the pros, depending on the metal wires used, a thermocouple is capable of measuring temperature in the range of -200 $^{o}$C to +2500 $^{o}$C. Thermocouples are rugged devices, meaning, they are immune to shock and vibration and suitable for hazardous environments. Thermocouples are small and have a low thermal capacity; they respond quickly to temperature changes, especially if the sensing junction is exposed. They can respond to rapidly changing temperature within a few milliseconds. Thermocouples require no excitation power, they are not prone to self-heating and are intrinsically safe.

The cons of using thermocouples - a substantial signal conditioning is necessary to convert the thermocouple voltage into a viable temperature reading. Signal conditioning requires a large investment in design time to avoid introducing errors that degrade accuracy. In addition to inherent inaccuracies in thermocouples due to their metallurgical properties, a thermocouple measurement is only as accurate as the reference junction temperature can be measured, approximately 1 $^{o}$C to 2$^{o}$C. Thermocouples consist of two dissimilar metals; in some environments, corrosion over time may result in deteriorating accuracy. Hence, thermocouples need great care and maintenance. When measuring microvolt-level signal changes, noise from stray electrical and magnetic fields can be a problem. Twisting the wire pair can greatly reduce magnetic field pickup. Using a shielded cable or running wires in metal conduit and guarding can reduce the electric field pickup. The measuring device should provide signal filtering.

As stated before, it is not easy measuring voltages generated by thermocouples into an accurate temperature reading. The voltage signal is small and the temperature-voltage relationship is non-linear. The most common thermocouple types are J, K, and T. At room temperature, their voltage varies at 52 μV/$^{o}$C, 41 μV/$^{o}$C, and 41 μV/$^{o}$C, respectively. Other thermocouple types have an even smaller voltage change with temperature.

**Table 4.1** Voltage Change vs. Temperature Rise (Seebeck Coefficient) for various Thermocouple Types at 25 $^{o}$C

| Thermocouple Type | Seebeck Coefficient (μV/$^{o}$C) |
|---|---|
| E | 61 |
| J | 52 |
| K | 41 |
| N | 27 |
| R | 9 |
| S | 6 |
| T | 41 |

Source: [15] Courtesy Analog Devices, Inc.

The principle on which thermocouples operate was discovered in 1821 by Thomas Johann Seebeck. Seebeck observed that, when two wires of dissimilar metals are joined in a closed circuit, an electromotive force (emf) is generated if the two junctions are maintained at different temperatures. This thermal emf induces an electric current to flow continuously through the circuit and is known as

Seebeck emf in honor of its discoverer [17]. Take two electrical conductors labeled A and B, whose junctions are exposed to different temperatures, $T_1$ and $T_2$. The thermal emf of this circuit, $E_{AB}$, is expressed by:

$$E_{AB} = f[A, B, (T_2 - T_1)] \tag{4.1}$$

$E_{AB}$, the thermal emf, is a vector quantity. Its magnitude and direction depend on the material characteristics of A and B as well as the temperature difference between the two junctions, $T_2 - T_1$, provided A and B are homogenous in composition.

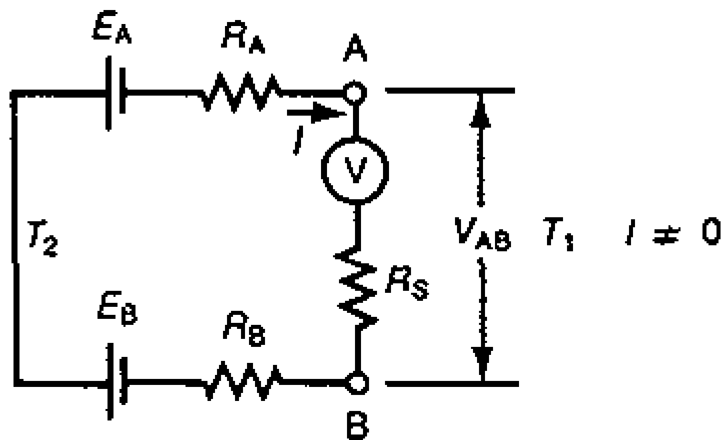


**Figure 4.2** A circuit diagram describing a thermocouple in a voltmeter circuit.
Source: [17] Courtesy of ASM.

Describing Figure 4.2; thermoelement A is represented by battery $E_A$ and resistance $R_A$. $E_A$ is the emf output of thermoelement A and $R_A$ is the resistance of

thermoelement A. Similarly, $E_B$ is the emf output of thermoelement B and $R_B$ is the resistance of thermoelement B. The voltage drop between the terminals of A and B is given by the following equation:

$$V_{AB} = E_A - E_B - I(R_A + R_B + R_S) \tag{4.2}$$

where $R_s$ is the resistance of the large resistor in series with the thermocouple to minimize the effect of the resistance of the thermoelements. If $E_A$ – ($E_A$ + $V_{AB}$) is positive, the thermoelectric current, I, will flow continuously from A to B. In this particular example, A is termed the positive thermoelement while B is the negative thermoelement of the thermocouple.

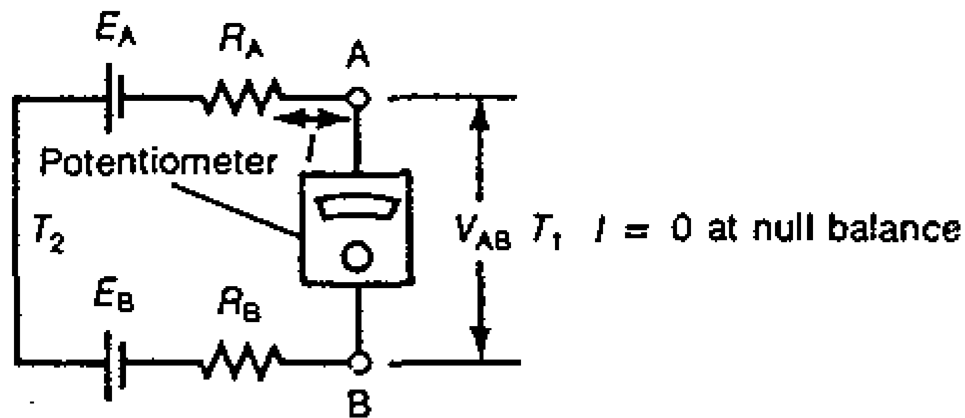


**Figure 4.3** A circuit diagram describing a thermocouple in a potentiometer circuit.
Source: [17] Courtesy of ASM.

In Figure 4.3, a potentiometer is connected across the terminals in place of the voltmeter. A bucking voltage is applied at the potentiometer until it is equal in

magnitude and opposite in direction to the thermoelectric voltage, $E_{AB}$. At null balance, there is no current flow. All the IR terms in equation 4.2 become zero. Under this condition:

$$V_{AB} = E_{AB} = E_A - E_B \tag{4.3}$$

The measured emf at the potentiometer $V_{AB}$ is the thermal emf of the thermocouple AB. It can be observed that thermal emf is a bulk property. It is independent of the resistance and hence, the diameter of the wire.

Thermoelectric power at a given temperature T is defined as the rate of change of thermal emf with respect to temperature. The thermoelectric power of the thermocouple AB at temperature T is the slope of its emf/temperature curve.

$$Thermoelectric\ Power = \frac{\Delta E}{\Delta T} \tag{4.4}$$

In using a thermocouple for temperature measurement, it is essential that the thermoelectric power of the thermocouple be fairly large and uniform within the applicable temperature range [18]. In case the emf/temperature relationship of thermocouple AB is well established, we may determine the temperature difference between $T_2$ and $T_1$ by measuring the generated thermal emf, $E_{AB}$, with

a potentiometer. The thermocouple does not measure the temperature of the junction $T_2$, but rather measures the temperature difference $T_2 - T_1$.

Thermocouples are separated into types based on their thermoelectric output. A type J thermocouple is widely used for its versatility and low cost. It consists of positive thermoelement iron and negative thermoelement 44Ni-55Cu alloy. The thermoelectric power of the type J thermocouple is about 55 μV/$^o$C. Type K thermocouples are also widely used in industrial applications. They consist of positive thermoelement 90Ni-9Cr alloy and a negative thermoelement 94% Ni alloy containing traces of silicon, manganese, aluminum, iron and cobalt. The thermoelectric power of a type K thermocouple is about 40 μV/$^o$C. For cryogenic measurements, a type T thermocouple is utilized. The positive thermoelement is copper and the negative thermoelement consists of 44Ni-55Cu. The positive thermoelement in a type E thermocouple is 90Ni-9Cr and the negative element is 44Ni-55Cu. The thermoelectric power of type E is the highest among all standard thermocouples. Type N is known as the Nicrosil/Nisil thermocouple. It was developed for oxidation resistance. The positive thermoelement is Nicrosil, which consists of 14 Cr, 1.4 Si, 0.1 Mg, bal Ni. The negative thermoelement is Nisil, which consists of 4.4 Si, 0.1 Mg, bal Ni. Type S thermocouples are widely used in industrial laboratories as a standard of calibration of base-metal thermocouples and other temperature sensing instruments. The thermoelectric output of a type S thermocouple is approximately 6 μV/$^o$C. The positive thermoelement in type S is Pt-10Rh and the negative thermoelement is high purity platinum. Type R thermocouples consist of a positive thermoelement Pt-13Rh and a negative

thermoelement of Pt. It is very similar to a type S but has a slightly higher emf. Type B thermocouples consist of positive thermoelement Pt-30Rh and negative thermoelement Pt-6Rh. Type B is less sensitive than type R or type S, but may be used in still air or inert atmospheres at temperatures approaching upwards of 1700 $^{o}$C [17].

# CHAPTER 5

# EXPERIMENTAL METHODS AND DATA ANALYSIS

## 5.1 Calibration via Blackbody Source

Every experiment requires calibration. The instruments utilized in these initial experiments were an IR-563 Blackbody source, an FLIR Camera EX- Series and a Laser Grip Model-1022. The setup was utilized to study the interaction of infrared radiation with various silicon wafers. The wafers varied in oxide thickness and orientation, their front side or back side. The IR-563 Blackbody was set in temperature intervals of usually of 50 $^{o}$C or 100 $^{o}$C, thus, using temperature of the Blackbody cavity as a control. The wafer was held by a clamping apparatus so that it would be positioned in front of the IR-563 Blackbody source. The FLIR camera was set to a proper emissivity and temperature measurements of various silicon wafers were made, while the infrared radiation was interacting with silicon – in transmission mode as well as reflection mode. A Laser Grip Model 1022 IR thermometer was used to verify the FLIR camera's findings. It must be noted here that the Blackbody source is a broadband source. No monochromatic source was used in these experiments.

**Table 5.1** FLIR Camera Where the Emissivity is Set to 0.7 and Laser Grip Model 1022 Where the Emissivity is Set to 0.7 Temperature Readings for a 150mm Silicon Wafer with an Oxide Thickness of 110nm and a Mass of 4.01g

| Temperature of the Blackbody ($^oC$) | Temperature readout of FLIR Camera ($^oC$) (ε = 0.7) | Temperature readout of Laser Grip Model-1022 ($^oC$) (ε =0.7) |
|---|---|---|
| 50 | 43.0 | 21.1 |
| 100 | 69.0 | 54.1 |
| 200 | 152.0 | 124.0 |
| 250 | 190.0 | 156.0 |
| 300 | 224.0 | 182.0 |

As can be seen from Table 5.1, there were many inconsistencies between the two temperature readouts, with the Laser Grip Model-1022 reading a temperature always lower than the FLIR camera while set at the same emissivity. Both instruments are highly sensitive to light and movement and the experimental setup was not ideal to combat these sources of error.

**Figure 5.1** Shows the experimental setup with the IR -563 Blackbody Source and clamping apparatus.

(a)

(b)

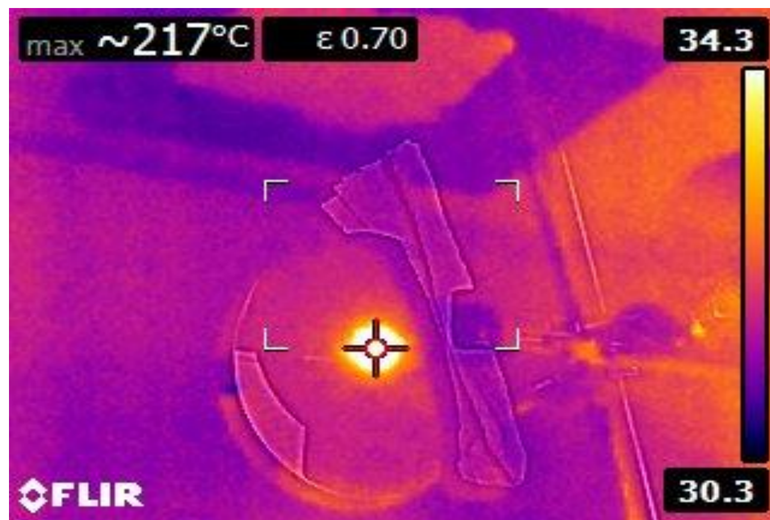


(C)

**Figure 5.2** Shows three different (a, b, c) infrared images obtained by the FLIR camera.

The infrared images shown in Figure 5.2 are obtained in a mode of the FLIR camera called hot spot. The hot spot is marked by the red crosshairs in the infrared images. These red crosshairs will always point to the highest temperature. The point with the highest temperature obtained by the crosshairs was the temperature noted for data in Table 5.1. The higher the temperature of the Blackbody cavity, the brighter the hot spot would glow, indicating an increase in temperature detected through the wafer.

The next experiment conducted was more complicated in depth and procedure requiring two wafers in alignment on the same clamping apparatus. The goal was to see how multilayers would affect the temperature read out. At first, the Blackbody cavity temperature was measured with the FLIR camera at an emissivity set at 1.0. Then each wafer was measured separately using the FLIR camera set at emissivity 0.7, front side and back side to compare differences. Then the two wafer temperatures, in alignment with one another, were measured using the FLIR camera at an emissivity of 0.7, taking into account both front sides and both back sides.

**Table 5.2** Temperature Measurements of Wafer #1 and Wafer #2 Separately Wafer #1 is a 0.7 mm Silicon Wafer with a 208nm Layer of Native Oxide ($SiO_2$) Wafer #2 is a 0.7mm Silicon Wafer with a 419nm Layer of Native Oxide

| T of Blackbody (°C) | T of Blackbody using FLIR (ε = 1) (°C) | T of Wafer #1 Front side (°C) | T of Wafer # 1 Back side (°C) | T of Wafer #2 Front side (°C) | T of Wafer #2 Back side (°C) |
|---|---|---|---|---|---|
| 50 | 62 | 47.1 | 47.1 | 48 | 48 |
| 100 | 69 | 51.9 | 51.4 | 52.2 | 52.2 |
| 150 | 104 | 66.4 | 63 | 67.5 | 66 |
| 200 | 120 | 74.3 | 75.4 | 79.5 | 79.4 |
| 250 | 161 | 89.4 | 87.7 | 96 | 97 |
| 300 | 188 | 105 | 106 | 114 | 115 |
| 350 | 210 | 122 | 120 | 129 | 131 |
| 400 | 267 | 152 | 152 | 158 | 163 |

At these temperatures, there is not much difference in the back side versus front side. Wafer #2 with its thicker oxide layer, in general, reads a higher temperature than Wafer #1 with its thinner oxide layer. It is obvious that, in the presence of a silicon wafer, the radiation from the Black body source is transmitted, reflected and emitted. Some of the radiation is turned into thermal energy read by the FLIR camera.

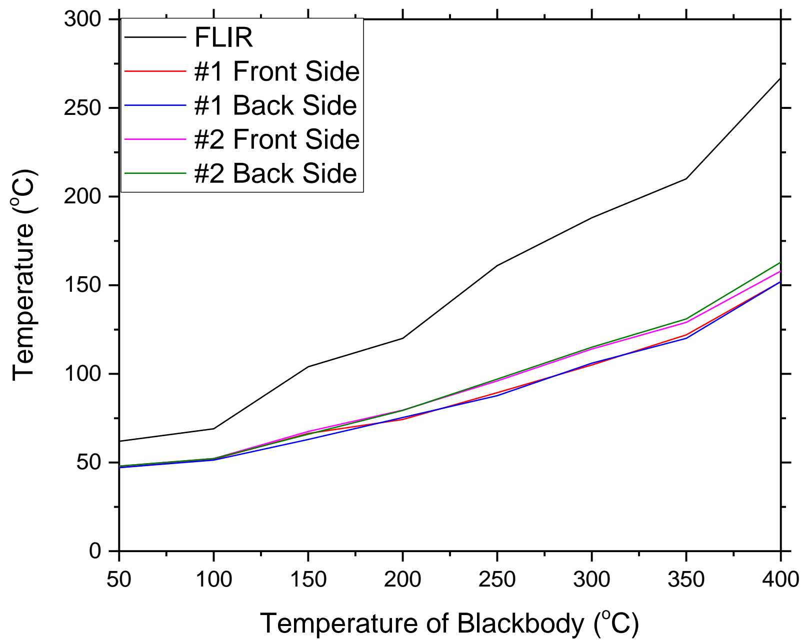


**Figure 5.3** Shows both wafer temperature measurements, front side and back side.

During these measurements, both wafers are in alignment with one another; the overall thickness of both wafers is much greater than the individual wafers. This thickness affects the temperature readouts.

**Table 5.3** Wafers #1 and #2 in Alignment with Measurements Taken with Respect to their Front and Back Sides

| T of Blackbody (°C) | T of Blackbody using FLIR (ε=0.7) (°C) | T of Wafer #1/#2 Front side (°C) | T of Wafer #1/#2 Back side (°C) | T of Wafer #2/#1 Front side (°C) | T of Wafer #2/#1 Back side (°C) |
|---|---|---|---|---|---|
| 50 | 62 | 57.3 | 43 | 44.1 | 44.1 |
| 100 | 69 | 44 | 43.5 | 43.8 | 43.5 |
| 150 | 104 | 47.3 | 47.3 | 47.3 | 47.3 |
| 200 | 120 | 52 | 52.4 | 50.3 | 52 |
| 250 | 161 | 58.4 | 58 | 56.4 | 55.8 |
| 300 | 188 | 65.8 | 66 | 66 | 65.8 |
| 350 | 210 | 72 | 72 | 73.5 | 72.7 |
| 400 | 267 | 85.5 | 83.1 | 83.5 | 80.5 |

At these temperatures, there is not much difference in the front side versus back side. There is a difference in the overall temperature readout. The wafers, in alignment, produce an overall thicker target for the incident radiation. The thicker target is shown to reduce the temperature obtained by the FLIR camera. This leads to more radiation being reflected and absorbed than transmitted through both wafers.

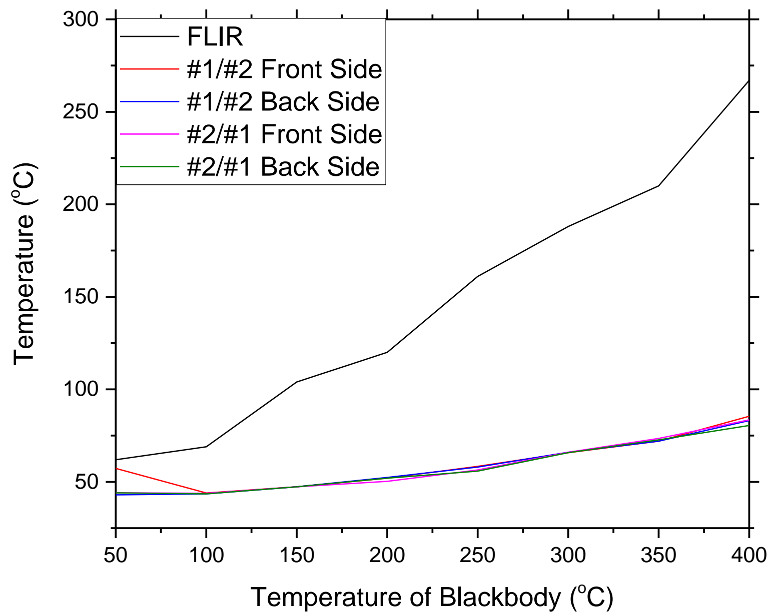


**Figure 5.4** Shows both wafers in alignment with each other during temperature measurement. There is a greater difference in temperature between the FLIR camera readout of the Blackbody and the single wafer versus the camera readout of the Blackbody and the layered wafers.

IR cameras use radiosity to approximate greybody emissivity. Radiosity is defined as the ratio of emitted to reflected radiant energy coming from a target and received by an IR camera.

$$L(T) = \int_{\lambda_1}^{\lambda_2} Pl(\lambda, T_{tgt} \varepsilon(\lambda) s(\lambda) \tau(\lambda, T_{atm}) d\lambda + \int_{\lambda_1}^{\lambda_2} Pl(\lambda, T_{bk} \big(1 - \varepsilon(\lambda)\big) s(\lambda) \tau(\lambda, T_{atm}) d\lambda \quad (5.1)$$

L(T) is the radiosity, Pl(λ,T) is Planck's function, T is temperature; tgt is target or object, bk is background, atm is atmosphere; ε(T) is the emissivity, s(T) is the detector and system optical response and τ(λ,T) is the atmospheric transmission, all at wavelength, λ [19].

For a greybody, approximating the radiosity, it is assumed that the emissivity is independent of wavelength; thus equation 5.1 can be written as:

$$L(T) = \varepsilon \int_{\lambda_1}^{\lambda_2} Pl\big(\lambda, T_{tgt}\big) s(\lambda) \tau(\lambda, T_{atm}) d\lambda + (1 - \varepsilon) \int_{\lambda_1}^{\lambda_2} Pl(\lambda, T_{bk}) s(\lambda) \tau(\lambda, T_{atm}) d\lambda \quad (5.2)$$

Combining equation 5.1 and 5.2, assuming now that $\tau(\lambda, T_{atm}) = 1$, for the measurement done close enough to the target, and solving for emissivity yields:

$$\varepsilon = \frac{\int_{\lambda_1}^{\lambda_2} [Pl(\lambda,T_{tgt}) - Pl(\lambda,T_{bk})]\varepsilon(\lambda)s(\lambda)d\lambda}{\int_{\lambda_1}^{\lambda_2} [Pl(\lambda,T_{tgt}) - Pl(\lambda,T_{bk})]s(\lambda)d\lambda} \quad (5.3)$$

This solution coincides with the algorithm used by IR camera manufactures to determine temperature and emissivity using the radiosity equation.

### 5.2 Multi-Rad

The simulations were performed using the software Multi-Rad. Multi-Rad was developed at Massachusetts Institute of Technology by Jeffrey P. Hebb, Justine Cave, David Wang, Shwan MacFarland, and Klavs F. Jensen. Multi-Rad uses thin film optics method for predicting the reflectance and transmittance of a multilayer thin film stack for a particular wavelength and angle of incidence. The thin film optics method treats the electromagnetic radiation as a wave; so it captures the interference effects in each layer [20]. The assumptions made for thin film optics are follows: the surface of the stack and all interfaces between films are optically smooth; the interfaces between the films are parallel; the dimensions of the sample in the direction parallel to the interfaces is much larger than the wavelength; the optical constants within a particular layer do not vary in the direction perpendicular to the interface. The thin film optics are implemented in a 2 x 2 matrix method of multilayers. Another assumption is that the materials are isotropic, which means the optical constants are not dependent on the crystallographic direction.

The equation is modeled for N layer interfaces and N+1 layers. $A_i$ and $B_i$ are the amplitudes of the forward and backward propagating electric field vectors on the left side of the interface, i. The prime notation on $A'_{N+1}$ and $B'_{N+1}$ indicates that these are amplitudes on the right side of interface N. Light is incident on interface 1, with angle of incident $\theta_1$. This is the central equation of multilayer theory relating the amplitudes on the left side of interface 1 with those on the right side of interface N:

$$\begin{pmatrix} A_1 \\ B_1 \end{pmatrix} = \left[\prod_{i=1}^{N} P_i D_i^{-1} D_{i+1}\right] \begin{bmatrix} A'_{N+1} \\ B'_{N+1} \end{bmatrix} = \begin{bmatrix} m_{11} & m_{12} \\ m_{21} & m_{22} \end{bmatrix} \begin{bmatrix} A'_{N+1} \\ B'_{N+1} \end{bmatrix} \tag{5.4}$$

where $P_i$ is the propagation matrix, $D_i$ is the dynamical matrix and $m_{ij}$ is an element of the transfer function matrix. The propagation matrix accounts for the effect of absorption and interference within a layer bounded by two interfaces. Layer 1 is not bounded by two interfaces; so the propagation matrix $P_1$ is set to equal the identity matrix. For layers 2, 3 …N, the propagation matrix is as follows:

$$P_i = \begin{bmatrix} e^{i\varphi_i} & 0 \\ 0 & e^{-i\varphi_i} \end{bmatrix} \tag{5.5}$$

where $\varphi_i = 2\pi \check{n}_i d_i \cos\theta_i / \lambda$ is the phase shift. The complex index of refraction is $\check{n}_i = n_i + ik_i$, where n is the index of refraction and k is the extinction coefficient. The

thickness of the layer is d, $\theta_i$ is the complex angle, and $\lambda$ is wavelength of the incident wave.

The dynamical matrix accounts for reflection and refraction at the interface i, relating amplitudes of the reflected and refracted waves on either side of the interface. The dynamical matrix is given according to the state of the polarization of the wave:

$$D_i = \begin{pmatrix} 1 & 1 \\ \check{n}_i cos\theta_i & \check{n}_i cos\theta_i \end{pmatrix} s\ wave \tag{5.6}$$

$$D_i = \begin{pmatrix} cos\theta_i & cos\theta_i \\ \check{n}_i & \check{n}_i \end{pmatrix} p\ wave \tag{5.7}$$

where s and p indicate that the electric field vector is perpendicular and parallel to the plane of incidence. Given the angle of incidence, the complex angles for the other layers are calculated in succession using the complex form of Snell's Law.

$$\sin\theta_{i+1} = \frac{\check{n}_i}{\check{n}_{i+1}} sin\theta_i \tag{5.8}$$

### 5.3 Simulation of Two Wafers with Different Thin Film Layers

These experiments were simulated with the aforementioned Multi-Rad program. The simulation consists of two silicon wafers both of 0.7mm in thickness. The

doping of the wafers will remain constant at the intrinsic doping of silicon which is $3.2 \times 10^5$ Ohm-cm. The temperature will remain constant at 650°C, the temperature of annealing. The wafers will contain two different layers, one of $SiO_2$, and one with $Si_3N_4$. The thickness of these thin film layers will be the main parameter in these simulations. Lastly, the front side and backside effects will be taken into account. Reflectance, transmittance and emittance will be evaluated. For reflectance:

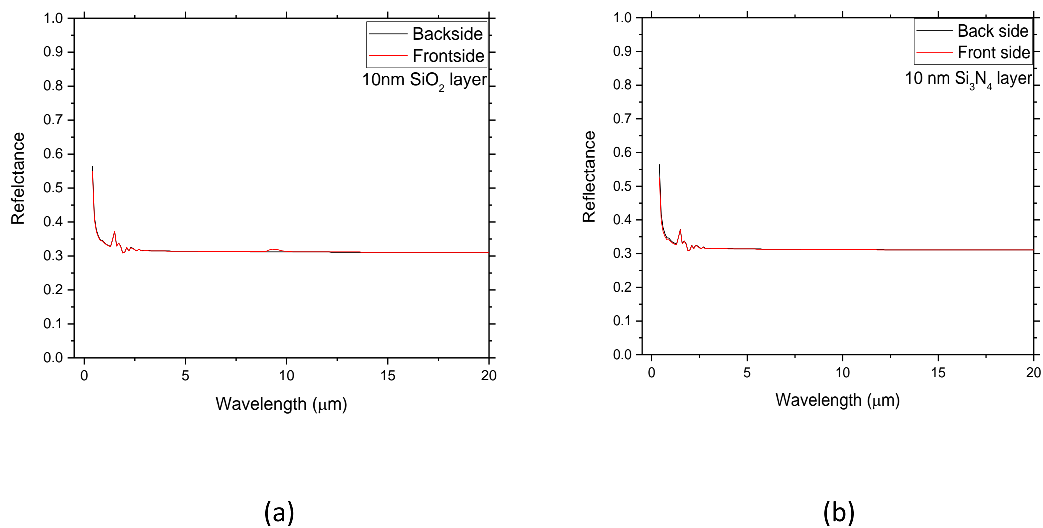


**Figure 5.5** Shows the Reflectance of two Silicon wafers (a) with 10nm $SiO_2$ oxide layer and (b) with 10 nm $Si_3N_4$ at 650 °C.

From Figure 5.5, it can be seen that there is not much difference between the two different thin film layers. Also, the front side back side effects show little difference. There is a very small thickness of film on these wafers. For a thicker layer of film, we obtain:

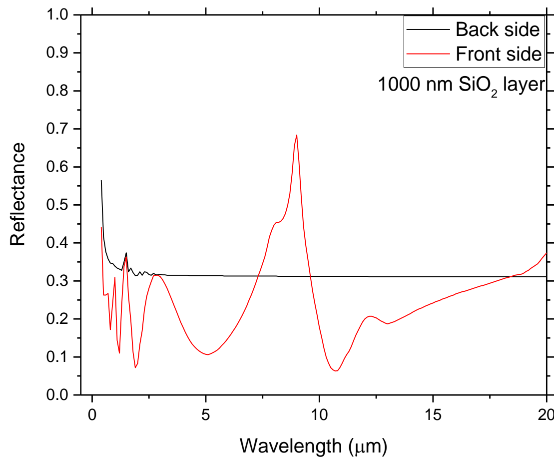


(a)

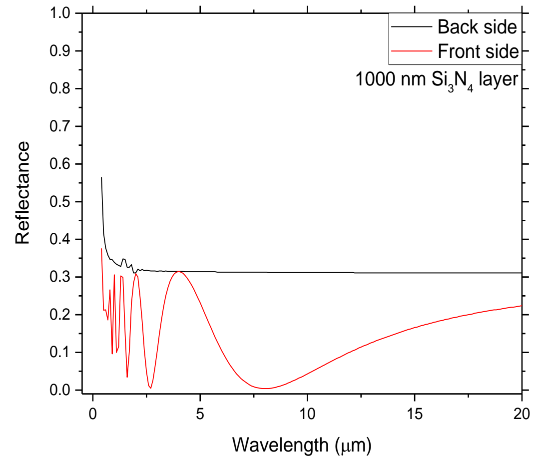


(b)

**Figure 5.6** Shows the Reflectance of two silicon wafers (a) 1000nm $SiO_2$ oxide layer and (b) 1000nm $Si_3N_4$ nitride layer.

From Figure 5.6, there is significant difference in the results of the $SiO_2$ and the $Si_3N_4$ layer. For this thicker thin film layer, the results for the front side (thin film layer closest to IR source) look much different from those for the back side (thin film layer farthest from IR source). The results for the back side look as if there is no thin film on the substrate and appear much like the 10nm thin film thickness sample. When examining the results for the front side, there are significant differences.

For transmittance, a new family of curves is produced. The transmittance is only significant for the 1-5 microns range of wavelengths. The results appear as in Figure 5.7.

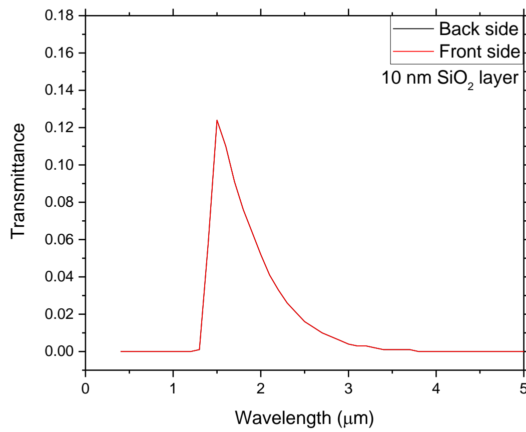


(a)

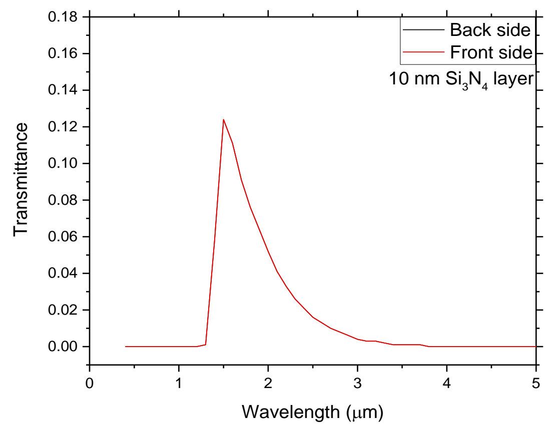


(b)

**Figure 5.7** Shows the Transmittance for two wafers (a) 10nm $SiO_2$ oxide layer and (b) 10nm $Si_3N_4$ nitride layer.

For this thin film, the peak transmittance, for the two wafers, appear to be identical. Their front side back side effects are negligible. For a thicker layer of film, we obtain:

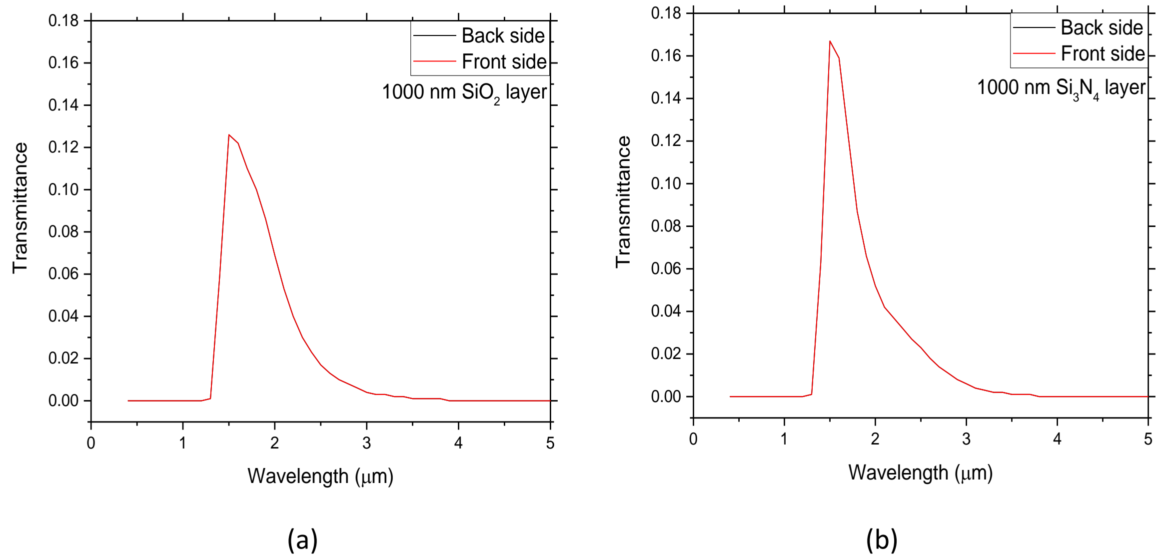


**Figure 5.8** Shows the Transmittance for two wafers (a) 1000nm $SiO_2$ oxide thickness and (b) 1000nm $Si_3N_4$ nitride thickness.

From Figure 5.8, we can see a difference in the results of the transmittance. The peak transmittance for $Si_3N_4$/Si is more than that of $SiO_2$/Si. Yet the font side back side effects for both wafers are negligible. Since the optical depth is kept constant, irrespective of the orientation of the wafer, the transmittance will remain the same for the front side and back side of the wafer [23].

Emissivity is an important parameter in semiconductor processing. It is defined as the ratio of the radiance of a given object to that of a blackbody at the same wavelength, temperature and surface conditions. One must know emissivity

to perform a proper temperature determination of an object [21]. For normal incidence, the emissivity, $\varepsilon(\lambda)$ of a plane-parallel specimen is given by:

$$\varepsilon(\lambda) = \frac{[1-R(\lambda)][1-T(\lambda)]}{[1-R(\lambda)T(\lambda)]} \tag{5.9}$$

where $\lambda$ is the wavelength, $R(\lambda)$ is the true reflectance and $T(\lambda)$ is the true transmittance. $R(\lambda)$ and $T(\lambda)$ can be related to the optical constants $n(\lambda)$ and $k(\lambda)$ by:

$$R(\lambda) = \frac{[n(\lambda)-1]^2+k(\lambda)^2}{[n(\lambda)+1]^2+k(\lambda)^2} \tag{5.10}$$

$$T(\lambda) = \exp[-\alpha(\lambda)t] = \exp\left[-\frac{4\pi k(\lambda)t}{\lambda}\right] \tag{5.11}$$

where $\alpha(\lambda)$ is the absorption coefficient and the t is the thickness of the material. From equation 5.9, it can be seen that, for an opaque body, when $T(\lambda) = 0$, from Kirchhoff's law the emissivity is [22]:

$$A(\lambda) = \varepsilon(\lambda) = [1 - R(\lambda)] \tag{5.12}$$

where, $A(\lambda)$ is the absorptance and $\lambda$ is the wavelength.

Effects such as light trapping and multiple internal reflections are dependent on the angle of incidence, surface roughness, interface roughness, etc. The experimentally measured apparent transmittance, T*(λ), and the apparent reflectance, R*(λ), are related to the true transmittance, T(λ), and the real reflectance, R(λ). They are given by the following equations:

$$T^*(\lambda) = T(\lambda)\,\frac{\left(1-R(\lambda)\right)^2}{\left(1-R(\lambda)^2 T(\lambda)^2\right)} \tag{5.13}$$

$$R^*(\lambda) = R(\lambda)\left\{1 + \frac{T(\lambda)^2\left(1-R(\lambda)\right)^2}{1-R(\lambda)^2 T(\lambda)^2}\right\} \tag{5.14}$$

Equations 5.13 and 5.14 are the result of considering multiple internal reflections.

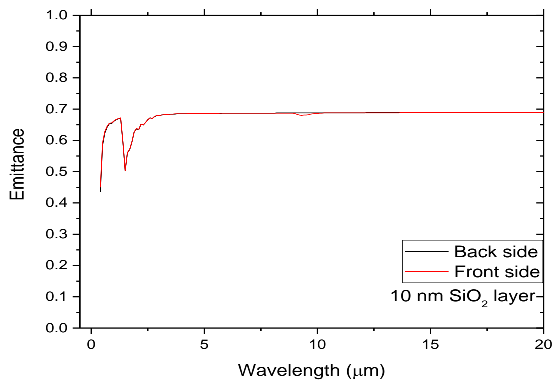


(a)

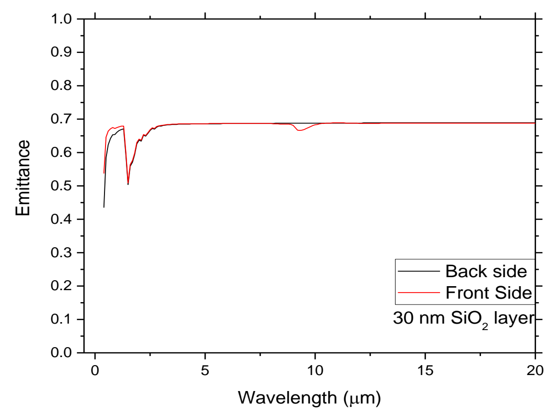


(b)

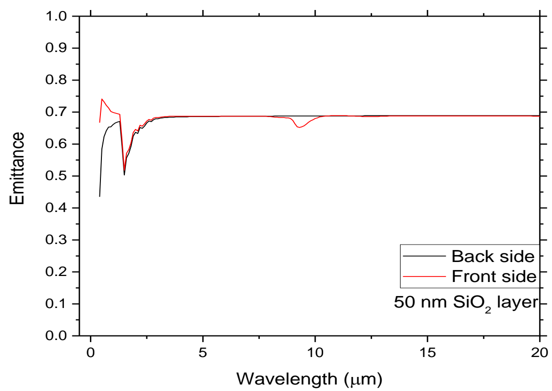


(c)

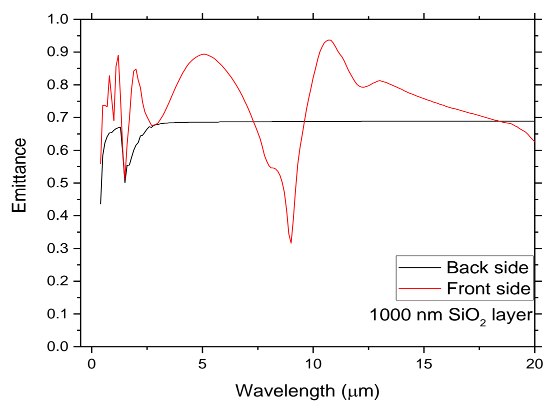


(d)

**Figure 5.9** Shows Emittance for various $SiO_2$ oxide thicknesses of (a) 10nm (b) 30nm (c) 50nm and (d) 1000nm.

From Figure 5.9, it can be seen that, as thickness increases, the front side back side effects become more important. For 1000nm thick films, the results for the front side are drastically different from those for the back side.

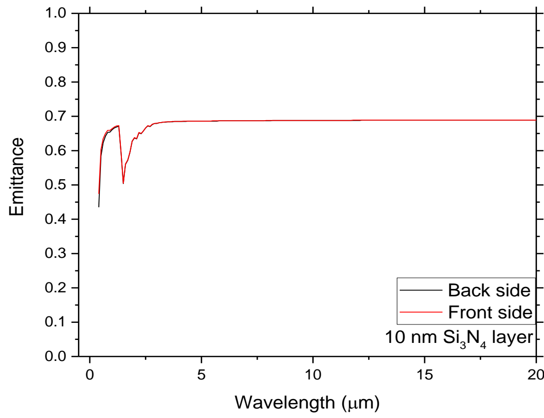


(a)

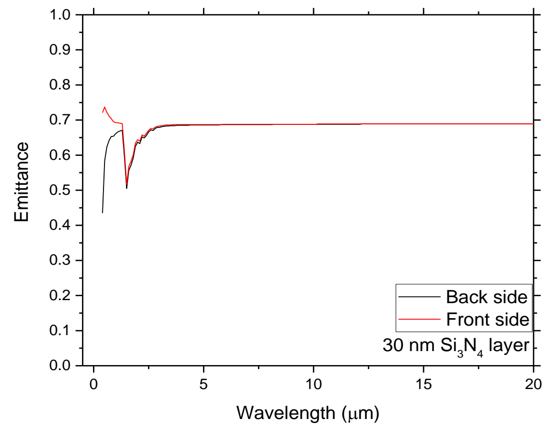


(b)

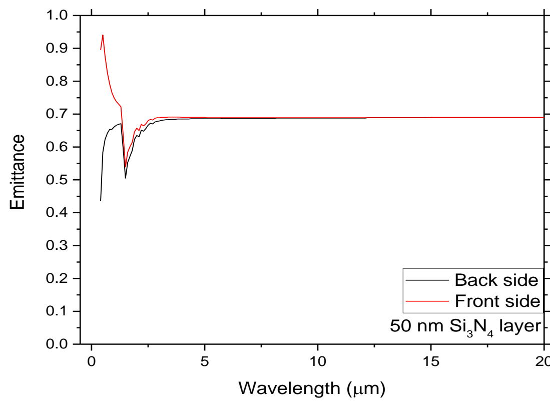


(c)

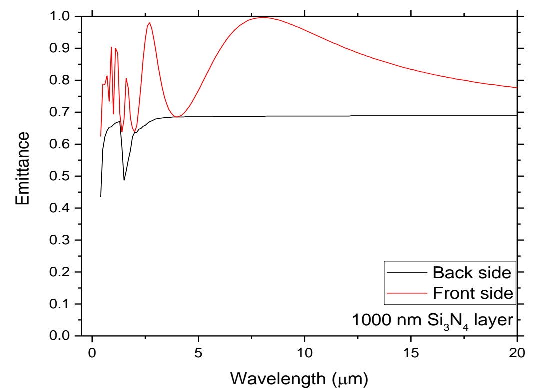


(d)

**Figure 5.10** Shows Emittance for various $Si_3N_4$ thicknesses of (a) 10nm (b) 30nm (c) 50nm and (d) 1000nm.

Figure 5.10 shows that, as nitride thickness increases, the front side back side differences become more prominent. For 1000nm nitride thickness, the results for the front side are drastically different from those of the back side.

For 1000nm thick films, the results also become more distinguishable between the $SiO_2$ and the $Si_3N_4$ as seen below:

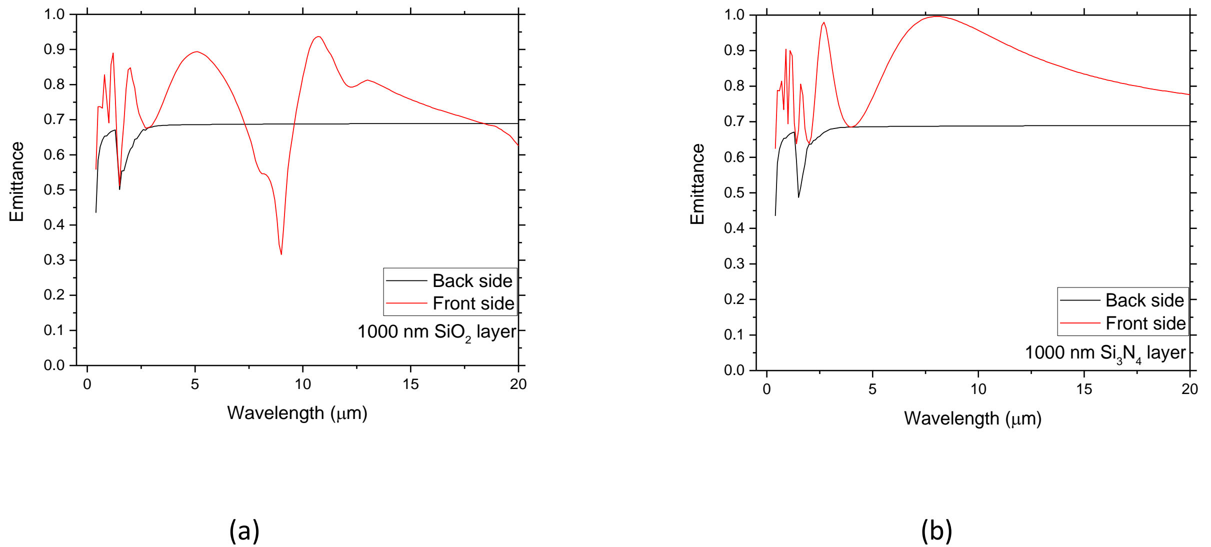


**Figure 5.11** Shows Emittance for both wafers with layers of, (a) $SiO_2$, and (b) $S_3N_4$ at 1000nm thickness.

Figure 5.11 shows that, for 1000nm film thickness, the front side of $SiO_2$/Si behaves much more differently from the front side of $Si_3N_4$/Si. The results for $Si_3N_4$/Si front side is always more than that for its back side. In contrast, the results for $SiO_2$/Si front side dip below its results for the back side for over a short range of wavelengths.

### 5.4 Simulation of SIMOX

SIMOX represents wafers that are processed by implantation of oxygen [Separation by ion IMplantation of OXygen] in silicon. The SIMOX wafer consists

of a layer of thin film silicon, a layer of buried silicon dioxide and the substrate layer of silicon. The simulations for the radiative properties of SIMOX were performed using the software known as Rad-Pro. Rad-Pro stands for radiative properties. It was developed by The Georgia Institute of Technology and National Institute of Standards [24]. The aforementioned Multi-Rad, which simulates radiative properties of silicon wafers with thin film coating, is limited in its approach when compared to Rad-Pro. Multi-Rad relies on pre-existing experimental data; its accuracy is limited to wavelength, temperature, and dopant concentration, which may not be always quite consistent and accurate. Rad-Pro allows users to predict the directional, spectral and temperature dependence of the radiative properties for the multilayer structures of silicon and related materials. Users can choose to use the formation for coherent, incoherent, and opaque substrates.

Since most silicon wafers are thick enough to be opaque in the wavelength range of 0.5μm and 1.0μm, the silicon substrate can be regarded as a semi-infinite medium. A wafer with a thin-film coating in the opaque region can be modeled as a multi-layer structure of thin films only. The transfer-matrix method can be used to calculate the radiative properties of a silicon wafer with thin films in the opaque region. Interferences in the silicon substrate are generally not observable from measurements because the wafer thickness is much greater than the coherent length. In this case, the incoherent formulation, or geometric optics should be used to predict the radiative properties of the substrate. To get rid of the fringes due to the thick substrate, the current version of Rad-Pro treats the thin film coatings as coherent, but the substrate as incoherent. The optical constants n, the refractive

index, and k, the extinction coefficient, of a material are complex functions of wavelength and temperature. They also depend on crystalline structure as well as doping levels. To calculate the optical constants of lightly doped silicon, whose dopant concentrations are less than $10^{15}$ $cm^{-3}$, carefully selected empirical expressions are used. On the other hand, the Drude model is employed to consider doping effects on the optical constants in silicon. Rad-Pro allows for the user to select the optical model of silicon between the empirical models for lightly doped silicon and the Drude model for doped silicon at any dopant concentration for a given dopant type.

When dealing with MOS transistors, one idealizes to high switching speed, high channel mobility, smaller short channel, and a lower kink effect. These electrical properties can be obtained by utilizing an ultra-thin silicon on insulator (SOI) layer [25]. One method to fabricate SOI wafers is to implant oxygen into the silicon called a separation by implantation of oxygen (SIMOX). The challenge in optical characterization of SIMOX is due to the built in multi-layers.

The SIMOX wafers contain a layer of thin film silicon as the top layer, a layer of buried silicon dioxide and a substrate of silicon. In this study, we consider the following parameters: the layer of thin film silicon is 200 nm thick; the layer of oxide is 400 nm thick and the silicon substrate is 0.7 mm thick. The thickness of the simulated SIMOX wafer remains constant throughout. The control in this simulation is the temperature. The temperature range investigated include: 30 $^{o}$C, 650 $^{o}$C, and 1300 $^{o}$C. The front side back side effects are compared. The optical properties of emittance, transmittance and reflectance are shown in Figure 5.12.

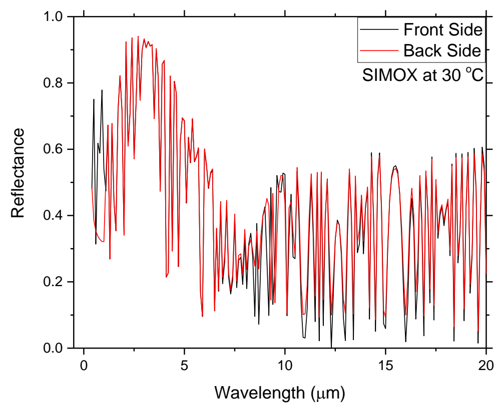


(a)

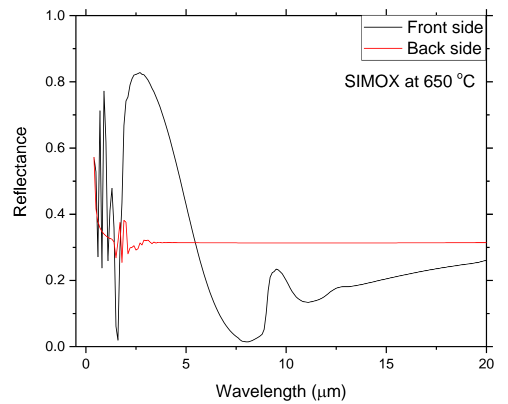


(b)

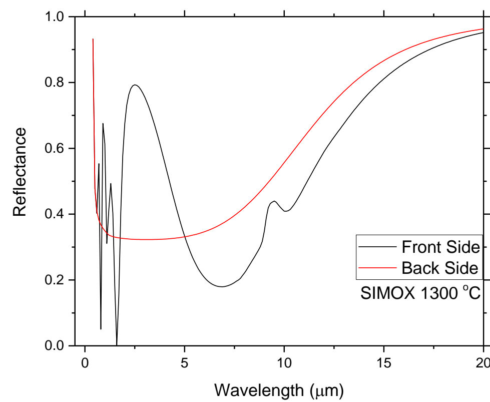


(c)

**Figure 5.12** Shows the Reflectance of front side vs. backside of SIMOX at:
(a) 30ºC, (b) 650ºC and (c) 1300ºC.

From Figure 5.12 (a), at 30 ºC, the front side back side effects are similar but vary at different wavelengths. For (b), at 650 ºC, the back side reflectance starts out varying in value and eventually settles to a mostly constant value over the wavelength range, while the front side differs significantly in value. For (c) at

1300 °C, both back side and front side reflectance are seen to change over the given wavelength, yet, the changes in reflectance of front side and back side differ.

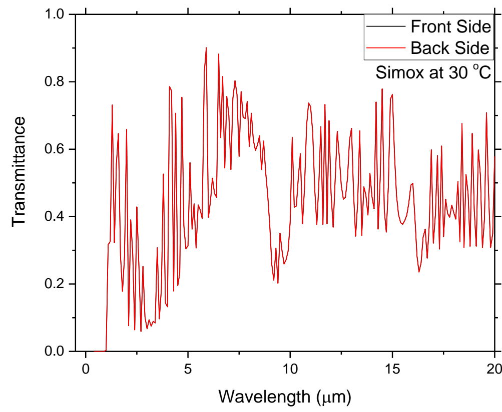


(a)

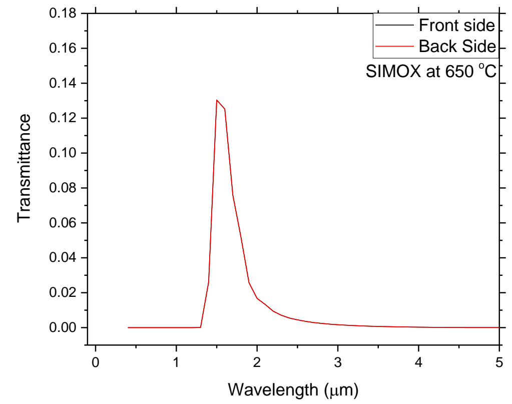


(b)

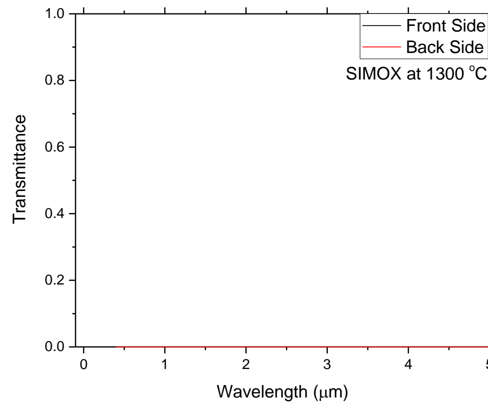


(c)

**Figure 5.13** The Transmittance of front side and back side of SIMOX at: (a) 30°C, (b) 650°C and (c) 1300°C. Note the transmittance range in (b) from 0.0-0.18.

Like in the previous simulation, using a wafer with a layer of $SiO_2$ and comparing it to a wafer with a layer of $Si_3N_4$, the front side and back side transmittance were always equal. The same is true for SIMOX when comparing front side and back side effects of transmittance; the two sides are optically equivalent (optical reciprocity). This is due to the fact that the thicknesses are the same throughout the experiment and the transmittance value is due to the thickness of the material. At 30$^oC$, (a) the transmittance varies significantly throughout the wavelength considered. At 650$^oC$, (b) the transmittance shows a nice peak. At 1300$^oC$, the transmittance is effectively zero. The transmittance decreases with increasing temperatures and becomes zero after 700$^oC$ for the entire wavelength range. The decrease in transmittance is due to silicon becoming intrinsic as a result of an increase in free carrier density with increasing temperature [25].

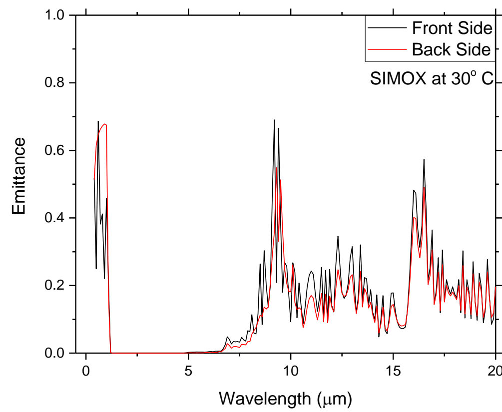


(a)

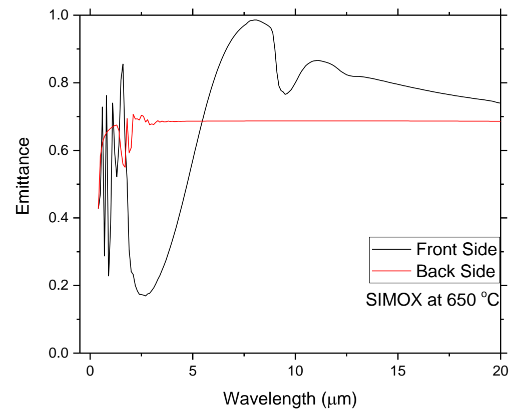


(b)

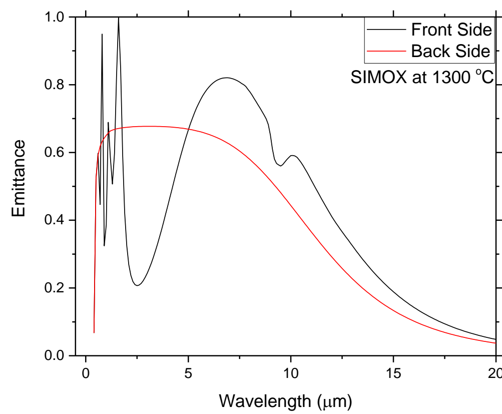


(c)

**Figure 5.14** The Emittance of front side and back side of SIMOX at: (a) 30°C, (b) 650°C and (c) 1300°C.

Figure 5.14 (a) shows the front side and back side emittance at 30°C. The front side and back side emittance change throughout the wavelength range. The

front side and back side emittance are not equal yet are close in behavior. For (b), at 650°C in Figure 5.14, the backside emittance varies in the shorter wavelength range and reaches a constant value as wavelength increases. The front side in (b) varies throughout the wavelength range. For (c), the front side and back side vary throughout the wavelength range. The front side and back side exhibit much different behavior from each other at 1300°C.

Many of the aforementioned optical phenomenon can be described in great detail using scattering theory. In the general case of incident radiation upon a medium, reciprocity theorem underlies the many assumptions and simplifications utilized to model the behavior, such as, monochromatic illuminations, finite size of scattering region, unique illumination, and detection direction. Reciprocity relates the input and output waves in pairs, irrespective of the presence or absence of other waves. When dealing specifically with electromagnetic wave propagation in a medium, the wave equation for an electric field is augmented with an index of refraction term [26].

$$\nabla^2 E = \left(\frac{n^2}{c^2}\right)\left(\frac{\partial^2 E}{\partial t^2}\right) + \left(\frac{\nabla n^2}{n^2}\ E\right) \tag{5.15}$$

Scattering can be characterized by a scattering amplitude derived from a scattering potential, F(r). This equation below is known as the scalar Helmholtz equation and is given by:

$$\nabla^2 E_i(r) + k^2 E_i(r) = -4\pi F(r) E_i(r) \tag{5.16}$$

The solution to the total field from a wave incident with wave vector k, with incident beam direction denoted by $\hat{s}_1$ and outgoing beam direction denoted by $\hat{s}_2$, and a scattering amplitude represented by $f(\hat{s}_2, \hat{s}_1)$, is given as:

$$E_1(r\hat{s}) = \exp[ik\hat{s}_1 \, . \, r\hat{s}] + \frac{f(\hat{s}_2, \hat{s}_1)\exp[ikr]}{r} \tag{5.17}$$

The simplest scope of optical reciprocity is to provide the transmission at normal incidence of collimated light through a stack of polarization changing elements. Transmission through each element can be described by its Jones matrix for coherent incident light. For incoherent incident light, the transmission can be provided by its Mueller matrix. A simple example of a Jones matrix for a linear polarizer combined quarter wave plate with a polarizing direction of 45° is given as:

$$M = \frac{1}{\sqrt{2}} \begin{pmatrix} 1 & i \\ 1 & i \end{pmatrix} \tag{5.18}$$

A Jones matrix of an optically active medium introduces a phase angle, δ, between right and left circularly polarized waves and is provided by:

$$M = \begin{pmatrix} cos\frac{\delta}{2} & sin\frac{\delta}{2} \\ -sin\frac{\delta}{2} & cos\frac{\delta}{2} \end{pmatrix} \quad (5.19)$$

An example of a Mueller matrix for incoherent incident light that propagates through a quarter wave plate facing along the vertical axis is given by:

$$M = \frac{1}{2}\begin{pmatrix} 1 & 0 & 0 & 0 \\ 0 & 1 & 0 & 0 \\ 0 & 0 & 0 & -1 \\ 0 & 0 & 1 & 0 \end{pmatrix} \quad (5.20)$$

Through reciprocity and coherence theory, Kirchhoff's law can be derived for all angles [27].

## 5.5 Comparison with the Literature

Sato has performed extensive studies on emissivity of silicon [28]. Sato's results of temperature and wavelength dependent emissivity are shown in Figure 5.15.

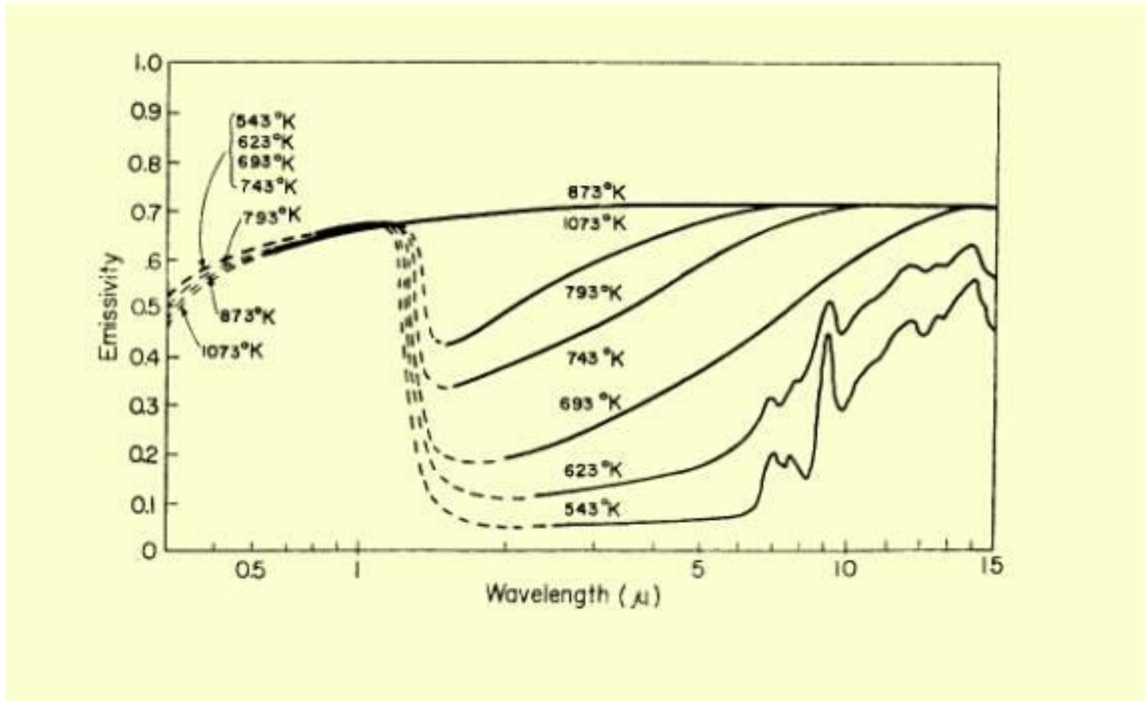


**Figure 5.15** Emissivity curves at different temperatures.

Source: [29].

The simulated results of emissivity of silicon, in this study, are consistent with those of Sato. Such comparisons with the emissivity of SIMOX, in the literature, lead to similar results.

# CHAPTER 6

# CONCLUSION

Radiative properties of silicon related materials have been presented in this study. Fundamentals of blackbody radiation and its applications to semiconductor processing have been described. Temperature measurement techniques such as thermocouples, imaging pyrometry in the form of infrared camera and single point infrared detector have been considered. Emissivity models in the form of Multi-Rad and Rad-Pro have been utilized to simulate the wavelength and temperature dependence of optical properties of silicon related materials and structures, in the wavelength range of 1 to 20 microns. Optical reciprocity has been examined for various case studies of layers on silicon substrates. The wavelength and temperature dependence of the radiative properties of SIMOX [Separation by ion IMplantation of OXygen] wafers have been examined.

## REFERENCES

1. Sarawat K.C., Chen Y-H, Khuri-Yakub B.T., Modeling, Measurement and Control of Rapid Thermal Processing, Transient Thermal Processing Techniques in Electronic Materials, The Mineral, Metals and Mining Society, pp. 1, 1996.

2. User's manual FLIR EX series, FLIR Systems Inc. pp. 38-47, 52-62, 2013.

3. Georgia State University, http://hyperphysics.phy-astr.gsu.edu/hbase/ems1.html, accessed February 18th 2016.

4. Siegel R., Howell J., Thermal Radiation Heat Transfer, 2nd ed., McGraw Hill, pp. 20-28, 1981.

5. http://quantumfreak.com/introduction-to-blackbody-radiation, accessed: Feburary,12th 2016.

6. Heald M. A., Where is the "Wein Peak"?, American Journal of Physics, Vol. 71, Issue 12, pp. 1322-1323, 2003.

7. http://sciencelearn.org.nz/var/sciencelearn/storage/images/contexts/light-and-sight/sci-media/images/refraction-of-light-in-water/685295-1-eng-NZ/Refraction-of-light-in-water.jpg, accessed: March, 12th 2016

8. Hummel R.E., Electronic Properties of Materials, 4th ed. Springer, New York N.Y, pp. 215-223, 2011.

9. https://upload.wikimedia.org/wikipedia/commons/thumb/a/a2/Damped sinewave.svg/2000px-Damped_sinewave.svg, accessed: March 12th, 2016

10. Lecture: Basic Semiconductor Physics, University of California Berkeley, EE105Fall2007Lecture1,http://www.inst.eecs.berkeley.edu/~ee105/fa07/lectures/Lecture%201.ppt, accessed: March 14th 2016.

11. Patel A., Radiative Properties of Silicon, New Jersey Institute of Technology, Newark, N. J, pp. 4-12, 1998.

12. http://www.thesolarspark.co.uk/wp-content/uploads/2013/02/Band-gaps.png, accessed: March 15th, 2016.

13. https://en.wikipedia.org/wiki/Direct_and_indirect_band_gaps, accessed: March 15th 2016.

14. Ghandhi S.K., VLSI Fabrication Principles, Silicon and Germanium Arsenide, 2nd ed., John Wiley & Sons, New York, N.Y, pp.3-13, 1994.

15. Duff M., Towey J., Two Ways to Measure Temperature Using Thermocouples Feature Simplicity, Accuracy and Flexibility, Analog Dialogue 44-10, pp. 1-6, 2010.

16. Delta Control Corporation, http://claustemp.com/thermocouple, accessed: March 16th 2016

17. Wang T.P., Thermocouple Materials, ASM Handbook, Vol. 2, Properties and Selections: Non-ferrous Alloys and Special Purpose Materials, ASM International, Materials Park, O.H, pp. 88-92, 1990.

18. Kreider K.G., DiMeo F., Platinum/Palladium Thin-Film Thermocouples for Temperature Measurements on Silicon Wafers, Sensors and Actuators, A 69, Gaithersburg, M.D, pp. 46-52, 1998

19. Madding R.P., Temperature Dependence of the Greybody Approximation to Emissivity for some Common Materials, Proceedings of SPIE Vol. 4710, Infrared training Center, FLIR Inc. pp. 37-43, 2002.

20. Hebb J.P., Pattern in Rapid Thermal Processing, Massachusetts Institute of Technology, Cambridge, M.A, pp. 81-89, 1997.

21. Ravindra N.M. et al., Emissivity Measurements and Modeling of Silicon Related Materials: An Overview, International Journal of Thermophysics, Vol. 22, No.5, pp. 1593-1611, 2001.

22. Ravindra N.M. et al., Modeling and Simulation of Emissivity of Silicon-Related Materials and Structures, Journal of Electronic Materials, Vol. 32, No.10, pp. 1052-1058, 2003.

23. Chen G., Borca-Tascuic T., Fair R.B., Photon Effect on Radiative Properties of Silicon During Rapid Thermal Processing, Journal of Applied Physics, Vol. 82, No.2, pp. 830-835, 1997.

24. Lee B.J, Zhang Z.M., Rad-Pro: Effective Software for Modeling Radiative Properties in Rapid Thermal Processing, 13th International Conference on Advanced Thermal Processing of Semiconductors, Georgia Institute of Technology, Atlanta, G.A, pp. 275-281, 2005.

25. Ravindra N.M. et al., Radiative Properties of SIMOX, IEEE Transactions on Components, Packaging, and Manufacturing Technology, Part A, Vol. 21, No. 3, pp. 441-449, 1998.

26. Potton R.J., Reciprocity in Optics, Institute of Physics Publishing, Reports on Progressing Physics, Rep.Prog.Phys.67, pp.724-729, 2004.

27. Greffet J.J., Niet-Vesperinas M., Field Theory for Generalized Bidirectional Reflectivity: Derivation of Helmholtz's Reciprocity Principle and Kirchhoff's Law, Optical Society of America, Vol. 15, No. 10, pp. 2735-2744, 1998.

28. Sato T., Spectral Emissivity of Silicon, Japanese Journal of Applied Physics, Vol. 6, No. 3, pp. 339-347, 1967.

29. http://pyrometry.com/images/semiconductors1.jpg, accessed: April 30th, 2016